

---

# Synthetic American Option Pricing via Jump-HMM-Driven Heston Implied Volatility

---

Julia Sun, Zheyu Jin, Jiawei Zhang, and Jeffrey D. Varner\*

Robert Frederick Smith School of Chemical and Biomolecular Engineering  
Cornell University, Ithaca, NY 14853  
{hhs68, zj276, jz2483, jd27}@cornell.edu

## Abstract

Generating realistic synthetic option prices requires implied volatility as an input, yet implied volatility is itself derived from observed option prices, creating a circular dependency that limits synthetic data availability for machine-learning and risk-analysis applications. We broke this circularity by developing a pipeline in which implied volatility emerged as an output of a structural model of equity returns rather than as an exogenous input. A Jump Hidden Markov Model produced multi-asset price paths with realistic stylized facts and cross-asset tail dependence; a modified Heston stochastic variance process whose mean-reversion target depended on regime state, days to expiration, moneyness, and an aggregate market-mood indicator converted those paths into implied-volatility paths; and a recombining binomial lattice priced American options from the resulting surface with early exercise. A central design choice was initializing the variance process at its mean-reversion target for each strike-expiration pair, so that the smile, skew, and term structure emerged automatically without external calibration. We calibrated the shape function through a hierarchy of representations spanning a parametric baseline, a globally shared neural surrogate, and a sector-specific neural surrogate fit to a multi-ticker, multi-sector option ladder. A temporal hold-out on a multi-day capture isolated scheduled corporate events as the dominant source of test-time generalization error, and calendar-derived earnings-distance and same-sector peer-coupling features fed to the shape network recovered the anticipatory portion of that signal. We then applied the calibrated framework as a synthetic-data generator on real near-the-money put and call contracts captured on one trading day, forward-simulating price paths under the JumpHMM and the per-ticker shape network and recovering path-conditional implied volatility, finite-difference American Greeks, and terminal short-premium profit and loss from one coherent simulation, and confirmed the cross-ticker robustness of the scenario by re-running the identical pipeline on a second underlying from a different sector and volatility regime. The framework was released as an open-source Julia package.

## 1 Introduction

Pricing American-style options requires implied volatility (IV) as an input, yet IV itself is an empirical quantity extracted from observed option prices [Black and Scholes \[1973\]](#). This circularity poses a practical problem for synthetic data generation: existing approaches either take IV from the market and feed it into a pricing model, or generate price paths without a consistent IV surface. Parametric IV models such as SABR [Hagan et al. \[2002\]](#) and the SVI parameterization [Gatheral](#)

---

\*Corresponding author.

[2004] treat the IV surface as an object to be fitted to market quotes, not generated from first principles; they produce smooth interpolations of observed smiles but cannot generate new IV dynamics for unobserved market conditions. Local volatility models Dupire [1994], Derman and Kani [1994] recover a deterministic volatility surface consistent with a single cross-section of option prices, yet the resulting surface is static and cannot produce the stochastic IV fluctuations observed in real markets. Stochastic volatility models such as Heston Heston [1993] generate realistic variance paths, but calibrating them requires observed option prices or IV as input, reintroducing the very circularity that the synthetic generator must avoid. The result is a gap in the literature: no existing framework generates self-consistent IV surfaces as an emergent output of a structural model of equity returns, without requiring observed option data as a calibration target during simulation.

This gap has practical consequences for a growing set of downstream applications. Empirical studies of IV surface dynamics Cont and da Fonseca [2002] have established that implied volatility exhibits rich cross-sectional and temporal structure, including smile curvature, skew, and term-structure effects that interact with market regimes. Reproducing this structure in synthetic data is essential for training machine-learning models that must generalize across market conditions, for backtesting hedging strategies such as deep hedging Buehler et al. [2019], and for conducting scenario-based risk analysis that requires consistent option prices across strikes and expirations. Historical resampling preserved realized distributional features Glasserman [2004] but could not produce out-of-sample tail scenarios consistent with a structural model of returns; generative approaches based on neural networks reproduced stylized facts of equity returns Wiese et al. [2020] but did not directly produce self-consistent option price and IV pairs. The scarcity of realistic synthetic option data therefore remained a binding constraint on progress in computational finance, particularly for studies that required option-level Greeks and path-conditional fair values rather than spot returns alone.

In this study, we addressed this gap by developing a framework in which IV was an *output* of a structural model of equity returns, not an input. The pipeline coupled a Jump Hidden Markov Model (JumpHMM) Alswaidan and Varner [2026] that produced multi-asset price paths with realistic heavy tails, negligible linear autocorrelation, and persistent volatility clustering Cont [2001], with cross-asset dependence imposed via a Student- $t$  copula Demarta and McNeil [2005]; a modified Heston stochastic variance process Heston [1993] that converted those price paths into IV paths, where the mean-reversion target  $\theta$  was a function of the HMM regime state, days to expiration (DTE), money-ness, and an aggregate market mood indicator; and a Cox-Ross-Rubinstein (CRR) binomial tree Cox et al. [1979] that converted the pre-computed IV into American option prices with early exercise. The central innovation was a hybrid  $\theta$ -function that linked the Heston mean-reversion target to the JumpHMM regime state, producing regime-dependent volatility dynamics. An equilibrium initialization  $v_0 = \theta(t = 0)$  gave each (ticker, strike, DTE) triple its own initial IV, so the smile, skew, and term structure emerged automatically without external IV data. Within this pipeline, the shape function that controlled the smile and term structure of  $\theta$  admitted a family of representations, and the modeling choice at each level of the family traded off model capacity for sharing across tickers. We therefore calibrated the shape function through a hierarchy of increasingly expressive forms: a parsimonious five-parameter functional form on single-ticker and cross-ticker semiconductor option chains, a globally shared neural surrogate that replaced the analytic form with a data-driven representation, and a sector-specific neural surrogate that let within-sector shapes specialize. The same decomposition supported a further relaxation to per-ticker networks once per-name sample sizes grew, without changing the downstream pipeline. We demonstrated this progression on a 31-ticker, fifteen-date, six-sector option ladder and on an eight-day temporal-holdout subset of the same capture, the latter of which isolated scheduled earnings events as the dominant source of the temporal generalization gap and motivated calendar-derived earnings-distance and same-sector peer-distance features that recovered a portion of that gap. The framework also produced realistic forward IV paths and American option prices with an endogenous crash-protection premium. The framework was implemented as an open-source Julia package designed to serve as a synthetic option market generator for downstream applications.

## 2 Background

The framework built on four established components, each contributing a distinct piece of the synthetic option generation pipeline: the JumpHMM produced realistic multi-asset price paths; the Heston stochastic variance process provided a mechanism for converting price dynamics into implied

volatility; a recombining binomial lattice translated IV into American option prices with early exercise; and a neural surrogate replaced the analytic shape function for the IV surface with a data-driven representation that absorbed sector-specific smile and term-structure geometry.

## 2.1 Jump Hidden Markov Model

The Jump Hidden Markov Model (JumpHMM) [Alswaidan and Varner \[2026\]](#) was developed for generating synthetic equity time series that simultaneously preserved three stylized facts of financial returns: heavy tails, negligible linear autocorrelation, and persistent volatility clustering [Cont \[2001\]](#). The model discretized continuous excess growth rates into  $N$  states via equal-probability quantile bins of a fitted Laplace distribution. The hidden state  $S_t \in \{1, \dots, N\}$  at each timestep governed the distribution of the excess growth rate  $G_t$ ; each state  $k$  emitted observations from a location-scale Student- $t$  distribution:  $G_t | S_t = k \sim \mu_k + \sigma_k \cdot t_\nu$ , where  $\mu_k$  and  $\sigma_k$  were learned per-state location and scale parameters and  $\nu$  was the shared degrees-of-freedom parameter. At each timestep, with probability  $\epsilon$  a Poisson( $\lambda$ )-distributed jump forced the chain into tail states (bottom or top  $N_{\text{tail}}$  states), creating sustained dwell periods in extreme-volatility regimes that produced the volatility clustering characteristic of empirical return series. For multi-asset generation, cross-asset dependence was imposed via a Student- $t$  copula [Demarta and McNeil \[2005\]](#) that preserved each asset’s marginal distribution while introducing realistic tail dependence; this copula structure ensured that joint tail events, in which multiple assets simultaneously occupied extreme states, occurred more frequently than a Gaussian copula would imply.

## 2.2 Heston stochastic variance model

The Heston model [Heston \[1993\]](#) specified the instantaneous return variance  $v$  of the underlying asset (i.e., the variance rate of its log-returns) as a mean-reverting square-root process:

$$dv = \kappa(\theta - v) dt + \sigma_v \sqrt{v} dW_v \quad (1)$$

where  $\kappa$  was the mean-reversion speed controlling how quickly the variance returned to its long-run level,  $\theta$  was the long-run variance target, and  $\sigma_v$  was the vol-of-vol governing the amplitude of stochastic fluctuations in  $v$ . In the standard formulation, the asset price and variance processes were coupled through a correlation  $\rho$  between their driving Brownian motions, producing the leverage effect in which negative returns coincided with rising volatility. The key property for our purposes was mean-reversion: the variance process was pulled toward  $\theta$ , so by controlling  $\theta$  we could control the equilibrium level of implied volatility. More generally, the Heston model produced a full European IV surface in  $(K, \tau)$  through its semi-closed-form characteristic-function pricing, and this analytic surface was the shape function that the neural surrogate below replaced in our pipeline. In the standard model  $\theta$  was a constant; our extension made  $\theta$  time-varying and state-dependent, linking it to the JumpHMM regime state, contract characteristics, and market conditions.

## 2.3 Lattice models for American options

Once the Heston shape function above supplies an IV per contract, the pipeline still needs to convert  $(S, K, \tau, r, q, \sigma)$  into an option price; for American options this rules out closed-form Black-Scholes and requires a numerical scheme. Lattice methods discretize the underlying-price process onto a recombining tree and price contingent claims by backward induction with an early-exercise check at each node [Broadie and Detemple \[1996\]](#). The Cox-Ross-Rubinstein (CRR) tree [Cox et al. \[1979\]](#) is the canonical construction, with up/down factors  $u = e^{\sigma\sqrt{\Delta t}}$ ,  $d = 1/u$ , and risk-neutral probability  $p = (e^{r\Delta t} - d)/(u - d)$ . Subsequent variants modified the moment-matching to address specific shortcomings of the CRR construction: Jarrow-Rudd [Jarrow and Rudd \[1982\]](#) matched the first two moments under the risk-neutral measure with  $p = 1/2$  at the cost of a non-zero log-drift term, Tian’s modified lattice [Tian \[1993\]](#) added a third-moment match to suppress the order- $\sqrt{\Delta t}$  pricing bias of the CRR tree, and Leisen-Reimer (LR) [Leisen and Reimer \[1996\]](#) replaced the moment-matching construction altogether with a Peizer-Pratt inversion of the binomial CDF, choosing  $p$  and  $u$  at each step so that the strike  $K$  landed on a tree node by design at every  $(S, \sigma)$  configuration. All four constructions converge to the Black-Scholes price as the number of steps increases, but their finite-step behavior differs sharply: the CRR price oscillates around the continuum limit because  $K$  drifts across node boundaries as  $\Delta t$  shrinks, the LR price converges monotonically because the strike is pinned to a node, and the Tian and Jarrow-Rudd trees fall in between [Leisen and Reimer \[1996\]](#),

Broadie and Detemple [1996]. The pinned-strike property of the LR construction also stabilizes finite-difference Greeks: small bumps to  $S$  or  $\sigma$  leave the strike on a node, so the staircase aliasing that CRR exhibits when the bump moves  $K$  across a node boundary is absent.

Two of these lattices appear later in this work and the choice between them is dictated by the use case. The pricing-pipeline pricer is the CRR tree at 200 steps: with IV pre-computed by the upstream Heston shape function, the pricer needs only a single  $\sigma$  input per contract, and CRR’s recombining structure makes the cost of pricing the full 234,549-row ladder linear in the number of steps. The forward-scenarios pricer, in contrast, required smooth Greeks at modest tree depth because the per-path scenarios in the §5 short-premium analysis computed  $\Delta$ ,  $\Gamma$ , and Vega by central finite differences against thousands of  $(S_t, \sigma_t)$  configurations along each simulated path; we therefore switched to the LR tree at 201 steps for that purpose, where the pinned-strike construction eliminated the bump-induced aliasing that CRR produced at the same depth. The pipeline did not depend on either choice in particular: any of the four lattices above would have been a drop-in replacement for the appropriate stage, and the decomposition between IV calibration and option pricing kept the choice of tree orthogonal to the rest of the framework.

## 2.4 Neural representations of the implied volatility surface

Parametric IV models such as SABR Hagan et al. [2002] and SVI Gatheral [2004] expressed the smile and term structure through low-dimensional closed-form functions, chosen to interpolate observed quotes while respecting no-arbitrage constraints. These forms were parsimonious and interpretable but inherited their expressive capacity from the chosen functional family, and a single global parameterization across a broad universe of tickers could not simultaneously accommodate sector-specific skew patterns and smile curvatures. A complementary line of work Horvath et al. [2021], Bayer and Stemper [2018] replaced the analytic form with a neural network that took  $(\ln \tau, \ln m)$  or a similar low-dimensional set of contract and model features as input and returned an IV or variance output; the network provided a flexible universal approximator for the shape of the surface while the downstream pricing pipeline remained unchanged. Neural surrogates of this kind have been used both as fast pricing approximators and as calibration targets in deep calibration schemes, and they admit the same multiplicative decomposition between a per-ticker level and a shared shape that the parametric forms use, making them a drop-in replacement for the functional form inside a generative pipeline. We used the neural surrogate in the structural sense rather than the deep-calibration sense:  $\psi_{\text{NN}}$  was the shape factor inside the multiplicative decomposition whose level  $v_t$  evolved with a JumpHMM-coupled Heston process, so the network supplied the cross-sectional geometry while the dynamics came from the generative model.

## 3 Methods

### 3.1 Pipeline overview

The generator produced synthetic American option prices through a three-stage pipeline:

$$\underbrace{\text{JumpHMM}(\text{prices})}_{\text{Stage 1}} \rightarrow \{S_t, s_t, \text{jumps}\} \rightarrow \underbrace{dv \text{ process}}_{\text{Stage 2}} \rightarrow \sigma_{\text{imp}} = \sqrt{v_t} \\ \rightarrow \underbrace{\text{CRR}(S_t, \sigma_{\text{imp}}, K, \text{DTE}, r_f)}_{\text{Stage 3}} \rightarrow P_{\text{american}} \quad (2)$$

This ordering was dictated by data flow: the JumpHMM produced the price paths and regime-state sequences that the Heston process required as inputs, and the Heston process produced the IV values that the CRR tree required for pricing. Each stage was self-contained, so the pipeline could be run forward without iteration or feedback from downstream stages.

### 3.2 Modified Heston variance process

We modified the standard Heston process (1) by making the mean-reversion target time-varying:

$$dv = \kappa(\theta(t) - v) dt + \sigma_v \sqrt{v} dW_v \quad (3)$$

The mean-reversion target decomposed into a per-ticker base level, an aggregate market mood modulator, and a contract-specific smile and term-structure adjustment that included a scheduled-event indicator:

$$\theta(i, t) = \theta_{i, s_t} \cdot (1 + \gamma \cdot M_t) \cdot \psi(\text{DTE}_t, K/S_t, e_{i,t}, e_{i,t}^{\text{peer}}) \quad (4)$$

where  $\theta_{i, s_t}$  was a per-ticker, regime-dependent variance level (one value per ticker  $i$  per HMM state  $s_t$ );  $\gamma \geq 0$  was the market mood sensitivity controlling how strongly aggregate stress elevated IV;  $M_t \in [0, 1]$  was the aggregate market mood; and  $\psi$  was the smile, term-structure, and event-shape adjustment with two earnings-event inputs  $e_{i,t}$  (signed days from  $t$  to ticker  $i$ 's nearest earnings print) and  $e_{i,t}^{\text{peer}}$  (the minimum of  $|e_{j,t}|$  over same-sector equity peers  $j \neq i$ ). The regime-dependent base  $\theta_{i, s_t}$  linked the Heston process directly to the JumpHMM state sequence for forward simulation: when the HMM transitioned into a tail state (via a Poisson jump or an extreme Markov transition),  $\theta_{i, s_t}$  rose, elevating the IV target. This mechanism produced the leverage effect as an emergent property of the return dynamics rather than as a separate model component: large negative returns drove the HMM into low-numbered tail states with  $p_{\text{neg}} \approx 0.52$ , which in turn elevated  $\theta$ . For the IV-surface calibration that follows, we restricted (4) to the operational form

$$\theta_{\text{cal}}(i, t) = \theta_i \cdot \psi(\text{DTE}_t, K/S_t, e_{i,t}, e_{i,t}^{\text{peer}}) \quad (5)$$

in which  $\gamma = 0$  (the aggregate mood multiplier was reserved for forward simulation with simulated state paths) and the per-state level  $\theta_{i, s_t}$  collapsed to a single per-ticker level  $\theta_i$  (since the calibration corpus consisted of observation-day IV surfaces rather than state-conditioned histories). Both restrictions were transparent to  $\psi$ , so the shape function carried over without modification when the full state-and-mood mechanism was reactivated for simulation.

The function  $\psi$  captured the shape of the IV surface with five parameters:

$$\psi(\tau, m) = \exp\left(\beta_1 \ln \tau + \beta_2 \ln m + \beta_3 \ln \tau \ln m + \beta_4 (\ln m)^2 + \beta_5 (\ln \tau)^2\right) \quad (6)$$

where  $\tau = \max(\text{DTE}, 1)$  and  $m = K/S$ . The parameter  $\beta_1$  controlled the linear term-structure decay;  $\beta_2$  controlled the skew (negative values produced put skew, with OTM puts having higher IV than OTM calls);  $\beta_3$  captured the DTE-skew interaction (the skew flattened at longer maturities);  $\beta_4$  controlled the smile curvature; and  $\beta_5$  controlled the DTE curvature, capturing the U-shaped ATM term structure where short-dated and long-dated IV were both elevated relative to intermediate maturities.

Rather than specifying a separate initial variance  $v_0$ , we initialized the variance process at its mean-reversion target:

$$v_0 = \theta(s_0, \text{DTE}, K/S_0, M_0) \quad (7)$$

This ensured that each (ticker, strike, DTE) triple started at its own equilibrium implied volatility. The initial IV surface inherited the smile, skew, and term structure encoded in  $\psi$  without requiring any external IV data. Different contracts on the same underlying received different  $v_0$  values, and the variance process immediately began mean-reverting around its local  $\theta(t)$ . The value of this design choice lay in eliminating  $v_0$  as a free parameter: the model did not require a separate calibration of the initial IV surface, as it was determined by construction from  $\theta$ .

The market mood  $M_t$  was defined as the fraction of tickers currently occupying tail HMM states, where  $N$  was the JumpHMM state count and  $N_{\text{tail}}$  denoted the number of extreme states at each end of the state space (inherited from the JumpHMM fit):

$$M_t = \frac{1}{N_{\text{tickers}}} \sum_{i=1}^{N_{\text{tickers}}} \mathbf{1}\left\{s_t^{(i)} \leq N_{\text{tail}} \text{ or } s_t^{(i)} > N - N_{\text{tail}}\right\} \quad (8)$$

This signal was fully endogenous to the JumpHMM copula model; it required no external data (e.g., VIX) and introduced no circularity. When multiple tickers simultaneously occupied tail states, the mood rose, elevating  $\theta$  and thus IV across all contracts, so that correlated IV spikes during market stress events emerged by construction. The variance process was discretized via Euler-Maruyama with a reflecting boundary at zero and a daily time step  $\Delta t = 1/252$ :

$$v_{t+1} = \left| v_t + \kappa(\theta_t - v_t)\Delta t + \sigma_v \sqrt{\max(v_t, 0)} \sqrt{\Delta t} Z_t \right|, \quad Z_t \sim \mathcal{N}(0, 1) \quad (9)$$

The reflecting boundary allowed  $\theta$  to vary freely across HMM states without requiring the Feller condition  $2\kappa\theta > \sigma_v^2$  to hold at every timestep Andersen [2008], a practical necessity since tail states

could drive  $\theta$  to values where the Feller condition would otherwise have been violated. American option prices were computed from the resulting IV using a CRR binomial tree with 200 steps per contract, a depth chosen because the price oscillation amplitude across that range fell below \$0.05 on the contracts of interest, well inside the bid-ask spread of the underlying market.

### 3.3 Neural surrogate for $\psi$

The parametric form of  $\psi$  in equation (6) used five shape parameters shared across all contracts on a given ticker. When the model was applied to a broad universe spanning multiple sectors, this global shape became a bottleneck: the semiconductor smile geometry differed systematically from mega-cap ETFs, healthcare names carried idiosyncratic event risk, and energy tickers inherited commodity-driven skew patterns not expressible by a five-term log-polynomial. We therefore replaced the parametric  $\psi$  with a neural surrogate Horvath et al. [2021], keeping the multiplicative decomposition  $\sigma_{\text{model}}^2 = \theta_{\text{ticker}} \cdot \psi$  but allowing the shape to be data-driven and adding two scheduled-event inputs ( $e$ ,  $e^{\text{peer}}$ ) that captured pre-earnings IV expansion and same-sector earnings spillover:

$$\psi_{\text{NN}}(\ln \tau, \ln m, e, e^{\text{peer}}) = \exp(\text{NN}(\tilde{z}_\tau, \tilde{z}_m, \tilde{z}_e, \tilde{z}_{e^{\text{peer}}})) \quad (10)$$

where each input was standardized to its training-set mean and standard deviation,  $\tilde{z}_x = (x - \mu_x)/\sigma_x$ . The earnings inputs were the signed clipped days-to-earnings for the contract’s ticker,  $e = \text{clip}(\Delta_{\text{earn}}^{(i)}, -30, 30)$ , and the minimum absolute days-to-earnings over same-sector equity peers excluding self,  $e^{\text{peer}} = \min_{j \neq i, c(j)=c(i)} |\Delta_{\text{earn}}^{(j)}|$  (clipped to 30). The peer feature carried the sector-coupling signal: a ticker  $j$  in the same sector printing on day  $t$  contributed  $e^{\text{peer}} = 0$  for all of  $i$ ’s contracts that day, which let the network learn the IV-spillover shape characteristic of the sector. For ETFs (no own earnings),  $e$  was set equal to  $e^{\text{peer}}$  taken over the full equity universe. The network produced  $\ln \psi$  so that  $\psi > 0$  by construction, preserving the log-Gaussian interpretation of the smile surface used in the parametric form. Each sector network was a two-hidden-layer multilayer perceptron with tanh activations:  $4 \rightarrow 16 \rightarrow 16 \rightarrow 1$  (369 parameters) for groups with  $\geq 2000$  observations and  $4 \rightarrow 8 \rightarrow 8 \rightarrow 1$  (121 parameters) for smaller groups, a width chosen to keep the observations-to-parameters ratio above 30 across all sector fits.

The decomposition defined a natural hierarchy of sharing. At one extreme, a single global  $\psi_{\text{NN}}$  shared across all tickers assumed that smile geometry was universal and left only the variance level  $\theta_{\text{ticker}}$  to distinguish names. At the other extreme, a per-ticker  $\psi_{\text{NN}}$  recovered ticker-specific shape but required enough data per name to resolve the surface without overfitting. We adopted a sector-specific intermediate: one  $\psi_{\text{NN}}^{(c)}$  per sector  $c$ , with all tickers within a sector sharing shape but each ticker retaining its own  $\theta_{\text{ticker}}$ . This choice reflected the empirical observation that within-sector tickers shared dominant risk factors (technology names tracked semiconductor cycles, healthcare names tracked FDA and trial catalysts, financials tracked rate expectations), so pooling shape across a sector provided a favorable bias-variance tradeoff at the current data volume. As per-ticker sample sizes grew, the same architecture supported relaxation to per-ticker networks without changing the downstream pipeline.

Training minimized the mean squared IV error jointly over the network weights and the per-ticker log-variance levels  $\{\ln \theta_{\text{ticker}}\}$ :

$$\min_{w, \{\ln \theta_i\}} \frac{1}{n} \sum_{i=1}^n \left( \sqrt{\theta_{t(i)} \cdot \psi_{\text{NN}}(\ln \tau_i, \ln m_i, e_i, e_i^{\text{peer}}; w)} - \text{IV}_{\text{market}, i} \right)^2 \quad (11)$$

where  $t(i)$  denoted the ticker of the  $i$ th observation. The log-variance levels were initialized from each ticker’s mean squared market IV and then updated jointly with the network weights under a single Adam optimizer, which coupled the level and shape fits and avoided the chicken-and-egg problem of fitting one conditional on the other. The learning rate followed a step schedule ( $1e-3 \rightarrow 5e-4$  at epoch 500  $\rightarrow 2e-4$  at 1000  $\rightarrow 1e-4$  at 1500), and training ran up to 2000 epochs with a best-checkpoint patience of 200 epochs on the training loss. Earnings dates were sourced from the public Yahoo Finance calendar and joined to each contract by ticker and observation date.

## 4 Calibration and Validation

### 4.1 Sector-specific neural calibration on the 31-ticker ladder

The parametric  $\psi$  of equation (6) provided the analytic starting point but assumed a single global smile and term-structure shape across all tickers, an assumption that became a bottleneck on a heterogeneous universe spanning sectors with structurally different risk profiles. To quantify the gap and the value of relaxing it, we collected full option ladders for 31 tickers spanning six sectors on fifteen capture dates between 2026-04-14 and 2026-05-11, producing 234,549 observations after filtering to moneyness  $K/S \in [0.80, 1.20]$ , non-zero bids, and  $IV \in (0.01, 2.0)$ . The sector partition followed conventional GICS-style groupings (Supplementary Table S1): technology (10 tickers), healthcare (8), financials (4), energy (3), retail (3), and broad-market ETFs (3). The corpus carried systematic cross-sector variation: mega-cap ETFs exhibited shallow smiles with pronounced term structure, technology names carried elevated near-term skew from earnings catalysts, healthcare names showed idiosyncratic bumps around trial and FDA dates, and commodity-linked energy tickers displayed skew patterns shaped by supply shocks rather than equity crash risk. Against this partition, we quantified the value of relaxing the global-shape assumption by fitting three nested models on the pooled ladder using a common loss (mean squared IV error) and a common level parameterization (one  $\theta_{\text{ticker}}$  per ticker), varying only the representation of  $\psi$ : a global parametric  $\psi$  with the five  $\beta$ -parameters shared across all tickers, a global neural  $\psi_{\text{NN}}$  shared across all tickers that replaced the parametric form with the neural architecture introduced in the methods, and a sector-specific neural  $\psi_{\text{NN}}^{(c)}$  with one network per sector. This design isolated the contribution of model capacity (parametric  $\rightarrow$  NN) from the contribution of sharing granularity (global  $\rightarrow$  sector).

We compared the three nested models on the pooled corpus and found that both axes contributed independently (Table 1): moving from the global parametric  $\psi$  to the global neural  $\psi$  reduced overall RMSE from 12.48% to 11.47% IV (an 8.1% relative improvement) by accommodating smile shapes the log-polynomial form could not express, and moving from the global to the sector-specific  $\psi_{\text{NN}}$  further reduced RMSE to 10.24% (a 17.9% cumulative relative improvement over the parametric baseline) by letting within-sector shapes specialize away from the global average. These figures were in-sample fits to the pooled corpus; a leave-one-date-out check that held out the latest capture and retrained on the remaining fourteen days produced a pooled test RMSE of 10.89% against a train RMSE of 10.21%, leaving a generalization gap of +0.68% IV (Supplementary Table S4) and confirming that the sector-NN result reflected faithful generalization rather than overfit to the multi-date pool.

Table 1: Three-way overall RMSE comparison on the 31-ticker ladder (234,549 observations across fifteen capture dates). The parametric baseline fit a single global set of five  $\beta$  parameters; the shared NN replaced the parametric  $\psi$  with one global network; the sector NN used one network per sector. All three models fitted one  $\theta_{\text{ticker}}$  per ticker jointly with the shape parameters.

Model	Overall RMSE (% IV)	Relative improvement vs. parametric
Parametric (5 $\beta$ , global)	12.48	(baseline)
Neural $\psi$ (1 network, global)	11.47	8.1%
Neural $\psi$ (6 networks, sector)	10.24	17.9%

The per-sector decomposition exposed where each incremental model capacity helped most (Supplementary Table S2). The global NN uniformly improved every sector over the parametric baseline, with the largest absolute gains in ETF (10.54%  $\rightarrow$  8.69%) and retail (11.73%  $\rightarrow$  10.23%), where the parametric log-polynomial struggled to fit shallow ETF smiles and idiosyncratic retail patterns simultaneously. Moving to sector-specific networks delivered a further 1 to 3% IV reduction in ETF, financials, retail, and technology but barely moved the needle in healthcare (12.71  $\rightarrow$  12.53%) and energy (8.24  $\rightarrow$  7.88%), reflecting cross-ticker dispersion in those sectors that a single shared  $\psi$  could not absorb even when freed from the parametric form. Technology remained the hardest fit overall (14.47% with sector NN); inspection of per-ticker residuals (Supplementary Table S3) traced this to heterogeneity within the sector itself rather than to a failure of the sector NN as a whole: within technology, names such as GOOG (9.57%), AVGO (9.94%), and NVDA (10.14%) fit comfortably under the shared Tech surface, while QCOM (21.46%), MU (18.45%), INTC (17.78%), and AMD (17.74%) pulled the sector RMSE upward. The pattern was consistent with these outlier

tickers carrying idiosyncratic smile shapes (elevated wings, asymmetric skew) that a shared Tech  $\psi$  could not simultaneously accommodate without degrading the fit of the better-behaved names. The same story repeated in healthcare, where ABBV (9.13%) and UNH (10.39%) fit well but PFE (17.66%), MRNA (17.49%), and AMGN (13.36%) drove the sector average. The per-ticker  $\theta_{\text{ticker}}$  values recovered a sensible IV level ranking: high-variance names with concentrated risk (INTC, MRNA, MU, AMD) occupied the top of the sorted order at 94 to 117% baseline IV, large-cap diversified names (AAPL, JPM, WMT) clustered near the middle at 46 to 52%, and the broad-market ETFs (SPY, QQQ, IWM) sat at the low-variance end near 35 to 42%. Within-sector clustering was evident in the sorted level estimates, confirming that sector membership captured a dominant axis of the cross-sectional IV structure.

Beyond the aggregate RMSE comparison, the residual structure under the sector NN was concentrated in the wings (moneyness below 0.90 and above 1.10) rather than near the money, consistent with the in-sample fits of the single-ticker baselines and with the known difficulty of pricing deep-OTM contracts where liquidity is thin and quoted IV is noisier. The learned  $\psi$  surfaces were smooth in both  $\ln \tau$  and  $\ln m$  and displayed the expected qualitative features, including put skew ( $\psi$  rising for moneyness below unity), smile curvature in the wings, and a mild term-structure gradient. The sector-to-sector differences in these surfaces motivated relaxing the global-shape assumption in the first place: the healthcare and technology surfaces curved more sharply in the near-term wings than the ETF surface, and the energy surface displayed a subtle asymmetry consistent with the commodity-linked risk profile of the sector. This calibration established the sector-specific neural  $\psi$  as the operating point of the framework on the pooled in-sample corpus, but the multiplicative decomposition supported a finer relaxation: one  $\psi_{\text{NN}}$  per ticker. We took up that extension on the same corpus below, where per-name sample sizes were large enough to fit per-ticker networks of the same architecture on nearly the full universe.

## 4.2 Per-ticker neural calibration on the pooled corpus

We trained one  $\psi_{\text{NN}}$  per qualified ticker on the full pooled corpus and recovered substantial within-sector detail that the sector network could not express (Fig. 1). The fifteen-date pooled corpus raised per-ticker sample sizes substantially over the original two-day capture, with twenty-nine of the thirty-one tickers clearing a 2,000-observation threshold sufficient to fit a  $\psi_{\text{NN}}$  of the same architectural family used at the sector level; the two unqualified tickers (PFE at 1,300 observations and BMY at 1,847) were held on the sector  $\psi_{\text{NN}}$  as a fallback so that every observation was priced under one or the other model. Network width followed sample size: tickers with at least 5,000 observations received the same  $2 \rightarrow 16 \rightarrow 16 \rightarrow 1$  architecture used for the sector networks, while smaller- $N$  qualified tickers used a  $2 \rightarrow 8 \rightarrow 8 \rightarrow 1$  network to keep the observation-to-parameter ratio above 20. The per-ticker  $\psi_{\text{NN}}$  reduced the pooled in-sample RMSE from 10.24% under the sector NN to 9.73% under the combined model (a 5.0% relative reduction) and improved twenty-one of the twenty-nine qualified tickers. The largest absolute gains were now spread across sectors rather than concentrated on a single one, with JNJ (11.14  $\rightarrow$  7.17%,  $-3.97\%$ ), MRNA (17.49  $\rightarrow$  13.74%,  $-3.76\%$ ), AAPL (14.30  $\rightarrow$  12.59%,  $-1.71\%$ ), INTC (17.78  $\rightarrow$  16.29%,  $-1.49\%$ ), AMGN (13.36  $\rightarrow$  12.14%,  $-1.22\%$ ), MU (18.45  $\rightarrow$  17.26%,  $-1.19\%$ ), and NVDA (10.14  $\rightarrow$  9.15%,  $-0.99\%$ ) all benefiting from a dedicated  $\psi$ . The improvement was visible at the level of the smile fit itself: on NVDA, the per-ticker  $\psi_{\text{NN}}$  tracked the steep put-skew gradient that the shared Tech surface flattened by averaging across MSFT and AVGO; on MSFT, the per-ticker network captured the gentler curvature near the money that the sector surface overshot; on LLY, the per-ticker fit followed the upward right wing that the Healthcare surface underweighted because of the shallower wings of the larger-cap healthcare names in the pool.

We translated the IV-RMSE story into a dollar-pricing story on the most recent capture (2026-05-11) by repricing each panel via 200-step CRR American at the IV implied by each calibration tier, and observed that the per-ticker  $\psi_{\text{NN}}$  collapsed dollar errors to within \$1 of market mid on liquid names while LLY carried a uniform IV-regime bias (Fig. 2). On SPY (DTE 7) and GS (DTE 11), the per-ticker  $\psi_{\text{NN}}$  sat inside the local bid-ask ribbon for 33% and 88% of contracts respectively, dominating both the parametric and sector tiers. On NVDA (DTE 7), all three model tiers clustered within  $\pm \$0.7$ , and the per-ticker fit matched the parametric form within the noise floor. LLY (DTE 11) showed a uniform positive bias of  $+\$2$  to  $+\$6$  across all three model tiers: the per-ticker  $\psi_{\text{NN}}$  encoded the time-averaged LLY IV across the fifteen capture dates, which included the 04-28 draw-down day when LLY's IV was elevated, so on a calmer day like 05-11 the static  $\psi$  overestimated

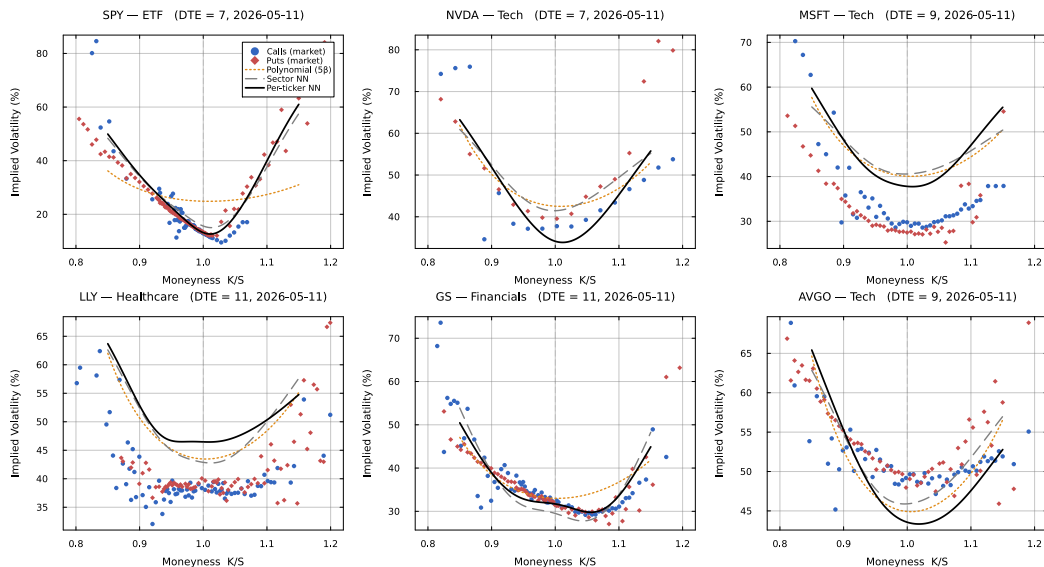


Figure 1: Per-ticker  $\psi_{NN}$  smile fits on the fifteen-date pooled corpus. Representative IV smile panels at mid-DTE for six qualified tickers spanning four sectors (SPY, NVDA, MSFT, LLY, GS, AVGO). The per-ticker network (solid black) tracked the smile shape more tightly than the sector network (dashed gray) on every panel, with the largest gap on NVDA and MSFT where the shared Tech surface flattened to accommodate AVGO’s elevated wings.

IV by several percentage points and the dollar error followed. The market-IV reference (yfinance-published IV repriced through CRR) sat at  $\sim \$0.6$  on LLY, confirming the CRR pipeline itself was sound and the residual was an IV-regime mismatch rather than a pricing error. The practical implication was concrete: on tickers whose realised IV on the sampled day matched the calibration-window average (SPY, NVDA, GS), the per-ticker  $\psi_{NN}$  delivered dollar errors at or below the bid-ask spread; on tickers whose sampled-day IV deviated from the average (LLY on 05-11), the static  $\psi$ ’s dollar error reflected the IV gap itself rather than a calibration failure.

The qualified set on the fifteen-date corpus covered the universe almost completely: only PFE (1,300 observations) and BMY (1,847) sat below the 2,000-observation cutoff, and both were healthcare names whose individual sample sizes remained the smallest in the pool. Within the qualified set, the eight tickers that did not gain over the sector NN (BAC, JPM, WFC, CVX, OXY, XOM, UPS, WMT) were concentrated in financials, energy, and retail—the sectors whose sector NN already absorbed most of the within-sector smile dispersion, leaving little residual structure for a per-ticker  $\psi$  to capture. This pattern set up the sample-size connection between per-ticker capacity and the temporal-generalization story below: the names that benefited least from per-ticker  $\psi_{NN}$  were also the names whose sector surface was already tight, while the names that gained most (JNJ, MRNA, AAPL, INTC, AMGN, MU, NVDA) sat in sectors with the largest residual within-sector dispersion. The temporal-generalization study itself used an earlier eight-day window from the same capture (2026-04-14 through 04-24) with a fixed train/test split, so that the holdout block was held apart from the pooled in-sample fits.

### 4.3 Temporal holdout and earnings-aware calibration

The pooled in-sample fit established that the sector-specific  $\psi_{NN}$  could absorb the cross-sectional smile geometry of the 31-ticker universe, but it left the temporal-generalization question unanswered: would a  $\psi$  trained on one block of capture days price contracts on a held-out subsequent block? To answer this, we used an eight-day subset of the pooled capture (2026-04-14 through 04-17 and 04-21 through 04-24, comprising 130,730 filtered observations) and split it into a six-day training block (04-14 through 04-22, 103,897 observations) and a two-day temporal holdout (04-23 and 04-24, 26,833 observations). The same 31 tickers appeared on every capture day, so the per-ticker  $\theta_i$  learned on the training block transferred directly to the holdout. We then asked a sharper question: which fraction of any test-set generalization gap was attributable to scheduled corporate

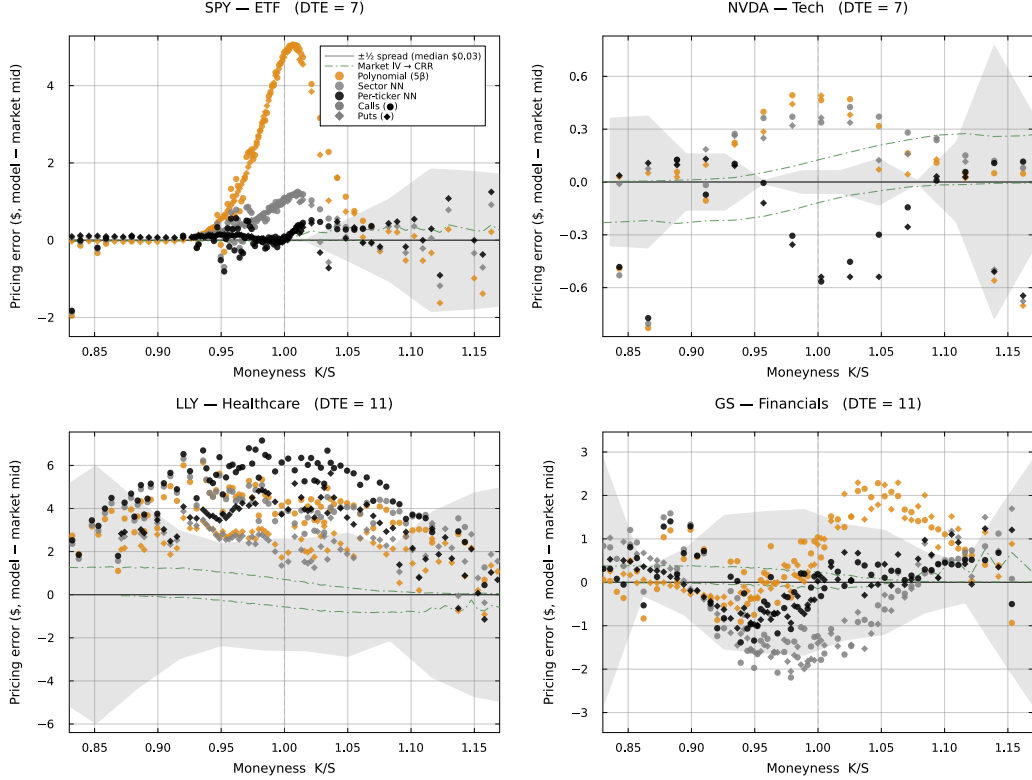


Figure 2: Model-vs-market dollar pricing error (CRR American at the calibrated IV minus market mid) versus moneyness for SPY (DTE 7), NVDA (DTE 7), LLY (DTE 11), and GS (DTE 11) on the 2026-05-11 capture. Four model tiers are overlaid on each panel: parametric  $\psi$  (light), sector  $\psi_{NN}$  (medium), per-ticker  $\psi_{NN}$  (dark), and market-IV reference (green dot-dash; yfinance IV repriced through CRR, near zero by construction). The gray ribbon was the local  $\pm \frac{1}{2}$  bid-ask spread band, computed per panel by partitioning the contracts into twelve equal-width moneyness bins, taking the median half-spread (ask – bid)/2 within each bin, and linearly interpolating the twelve bin values onto a fine moneyness grid. A point falling inside the band was a model error smaller than the typical bid-ask spread at that moneyness, i.e., a price within the range the market itself was quoting; the band widened toward the wings because bid-ask spreads were systematically larger for deep in- and out-of-the-money contracts. The per-ticker fit dominated parametric and sector tiers on SPY and GS, matched them on NVDA, and showed a uniform positive bias on LLY consistent with the per-ticker  $\psi$  encoding the time-averaged IV across fifteen capture dates and the sampled day (05-11) being calmer than the calibration-window average.

events embedded in the holdout window rather than to architectural overfit? To separate these contributions, we ran the sector  $\psi_{NN}$  under three configurations: (A) a pooled control identical to the in-sample architecture above (two inputs  $\ln \tau$ ,  $\ln m$ , no exclusion); (B) a non-earnings baseline that excluded all training and test rows for which the row’s ticker or any same-sector peer was within  $\pm 3$  days of an earnings print; and (C) the earnings-aware model introduced in the methods that fed  $\psi$  four inputs ( $\ln \tau$ ,  $\ln m$ ,  $e$ ,  $e^{\text{peer}}$ ) and used the same train and test rows as the control. The peer feature carried sector-coupling information directly: for any ticker  $i$  on day  $t$ ,  $e^{\text{peer}}$  collapsed to zero if any same-sector equity printed earnings that day, regardless of  $i$ ’s own distance to its next print.

The three-way comparison resolved the generalization question (Table 2). Configuration B revealed that scheduled earnings events accounted for the entire test-time generalization gap of the sector NN: with all earnings-window observations removed from both splits, the test RMSE (7.96%) fell to within rounding of the train RMSE (8.02%), giving a generalization gap of  $-0.06\%$  IV. The architecture itself generalized faithfully out of sample; what failed was the model’s ability to price options on days when an earnings catalyst dominated the IV surface. Configuration C confirmed that adding event-aware inputs to the shape network recovered roughly one-fifth of the lost perfor-

Table 2: Temporal-holdout sector-NN comparison across the three configurations. The pooled control (A) reproduced the existing four-day reference number (13.03% test RMSE on the same train/test split). Excluding earnings-window observations from both train and test (B) reduced the test RMSE to 7.96% and collapsed the generalization gap from +4.99 to  $-0.06\%$  IV. Adding the earnings indicator and peer-coupling feature to the input vector (C) on the original train and test rows reduced the pooled test RMSE to 11.98% and the generalization gap to +4.36%.

Configuration	$N_{tr}$	$N_{te}$	Train (%)	Test (%)	Gap (%)
A: pooled (2-input)	103,897	26,833	8.05	13.03	+4.99
B: non-earnings (2-input)	29,383	4,516	8.02	7.96	$-0.06$
C: earnings-aware (4-input)	103,897	26,833	7.61	11.98	+4.36

mance: relative to the pooled control, the test RMSE dropped from 13.03% to 11.98% (1.05% IV absolute, 8.1% relative), and the generalization gap narrowed from +4.99 to +4.36%. The peer-coupling feature did the heavy lifting in this reduction: the per-ticker breakdown showed the largest improvements on Tech names whose own earnings prints fell outside the immediate holdout window but whose sector peers printed during it (Supplementary Table S5). QCOM (own print 6 days after the holdout) and AMD (12 days after) both benefited from the peer-coupling signal because INTC printed inside the window and dragged their IV surfaces with a  $\sim 4\%$  IV reduction in test error each. The same mechanism reduced META, MSFT, and GOOG test RMSE by 2 to 4% IV apiece. INTC itself, the print-day ticker, was the one Tech name whose RMSE rose under the earnings-aware fit (33.17  $\rightarrow$  35.94%); its outsized +2192% EPS surprise produced an unanticipated post-print IV crush that no scheduled-event indicator could predict from the calendar alone.

These results set the limit of what a calendar-driven event indicator can and cannot do. The limit was sharp: the indicator captured the part of event-day IV behaviour known in advance from the calendar (pre-earnings IV expansion on the reporting ticker, sympathy moves on same-sector peers), but it carried no information about the post-event direction or size of the IV move when the actual print deviated from consensus. The non-earnings baseline of Configuration B was therefore the right reference point against which to compare future event mechanisms: any extension of the model aimed at pricing event-day IV surfaces had to be evaluated against the 7.96% non-event RMSE rather than against the pooled 13.03%, because that gap quantified the residual event signal the current architecture could not reach. We return to this distinction in the discussion, where the failure of the indicator on INTC and its success on the sympathy peers motivate a per-ticker tail mechanism reserved for future work.

## 5 Forward-simulated short-premium scenarios

We forward-simulated 1,000 Goldman Sachs (GS) price paths over a 31 trading-day horizon and observed that the model’s  $t = 0$  Leisen-Reimer fair value sat essentially at the market mid on both legs (put: \$17.26 vs. \$16.51, edge +\$0.75; call: \$16.07 vs. \$16.09, edge  $-\$0.02$ ; Supplementary Table S6). The two contracts were real GS options pulled directly from the 2026-04-28 ladder capture: a short put at  $K_p = \$890$  (market  $\Delta = -0.295$ , mid \$16.51, market IV 31.3%) and a short call at  $K_c = \$970$  (market  $\Delta = +0.328$ , mid \$16.09, market IV 28.9%), both expiring 2026-05-29 with the underlying spot at  $S_0 = \$926.38$ . Each path drew from the JumpHMM marginal pretrained on GS returns. Conditional on the path, we evolved a Cox-Ingersoll-Ross variance level  $v_t$  with mean-reversion  $\kappa = 2.0$ , vol-of-vol  $\sigma_v = 0.5$ , and leverage coupling  $\rho = -0.6$ , and at every trading day along every path we re-priced both contracts via 201-step Leisen-Reimer American with  $\sigma_t^2 = v_t \cdot \psi_{NN}((K/S_t)_{std}, (T-t)_{std})$ , the per-ticker neural smile/term-structure surface from the ladder calibration. We adopted Leisen-Reimer over the standard CRR lattice because the Peizer-Pratt construction places the strike  $K$  at a fixed lattice position by design at every  $(S, \sigma)$  configuration, which gave smooth Greeks via finite differences without the staircase aliasing that CRR’s recombining tree produced when bumps moved  $K$  across node boundaries. The seller received the market mid as the entry premium, and the model marked the position to its Leisen-Reimer fair value at every subsequent step; we assumed no scheduled earnings event during the 31-day window so the only sources of variation were diffusion, jumps, and the variance dynamics themselves. With the

entry edge near zero, the simulated short was being sold at par with the model’s own fair value at the entry capture and the realised path-conditional P&L could be read directly as a return.

The forward-simulation engine is summarised in Algorithm 1. Each simulated trading day along each path produced a  $(S_t, \sigma_t)$  pair from which the LR pricer returned a fair value for the contract; the same  $(S_t, \sigma_t)$  pair fed Supplementary Algorithm 2 for the central finite-difference Greeks. The two algorithms shared the lattice constructor and the per-ticker  $\psi_{\text{NN}}$  surface, so the Greek bumps inherited the same shape function used for the base mark and did not require a separate calibration.

---

**Algorithm 1** Forward simulation of path-conditional option premia

---

**Require:** JumpHMM marginal for ticker  $i$ ; per-ticker  $\psi_{\text{NN}}^{(i)}$  and level  $\theta_i$ ; contract  $(K, T)$ ; CIR parameters  $(\kappa, \sigma_v, \rho)$ ; spot  $S_0$ ; risk-free rate  $r$ ; number of paths  $N_p$ ; LR tree depth  $N_{\text{LR}}$ ; step  $\Delta t = 1/252$ .

**Ensure:**  $\{S_t^{(j)}, v_t^{(j)}, \sigma_t^{(j)}, P_t^{(j)}\}$  for  $j = 1, \dots, N_p$  and  $t = 0, \dots, T$ .

```

1:  $v_0 \leftarrow \theta_i \cdot \psi_{\text{NN}}^{(i)}(\ln(K/S_0), \ln T)$  ▷ equilibrium initialization, eq. (7)
2: for  $j = 1$  to  $N_p$  do
3:   Draw price path  $\{S_t^{(j)}\}_{t=0}^T$  from the JumpHMM marginal
4:    $v_0^{(j)} \leftarrow v_0$ 
5:   for  $t = 0$  to  $T - 1$  do
6:      $\sigma_t^{(j)} \leftarrow \sqrt{v_t^{(j)} \cdot \psi_{\text{NN}}^{(i)}(\ln(K/S_t^{(j)}), \ln(T - t))}$ 
7:      $P_t^{(j)} \leftarrow \text{LR}_{N_{\text{LR}}}(S_t^{(j)}, K, \sigma_t^{(j)}, T - t, r)$  ▷ Leisen-Reimer American
8:     Draw  $Z_S^{(j)}$  from the JumpHMM return innovation; draw  $Z_\perp \sim \mathcal{N}(0, 1)$  independent
9:      $Z_v^{(j)} \leftarrow \rho Z_S^{(j)} + \sqrt{1 - \rho^2} Z_\perp$  ▷ leverage coupling
10:     $v_{t+1}^{(j)} \leftarrow |v_t^{(j)} + \kappa(\theta_i - v_t^{(j)}) \Delta t + \sigma_v \sqrt{\max(v_t^{(j)}, 0)} \sqrt{\Delta t} Z_v^{(j)}|$ 
11:  end for
12:   $P_T^{(j)} \leftarrow \max(\phi(S_T^{(j)} - K), 0)$  ▷  $\phi = +1$  call,  $\phi = -1$  put
13: end for
14: return  $\{S_t^{(j)}, v_t^{(j)}, \sigma_t^{(j)}, P_t^{(j)}\}$ 

```

---

We rendered the share-price ensemble alongside the short-put and short-call premium ensembles (Fig. 3). On the worst-5% paths (red, top row), GS drifted toward and through  $K_p$ , the short-put premium climbed many-fold above its entry price, and the position closed with a mean P&L of  $-\$113.66$  on those paths. On the top 1–5% paths (green, bottom row; the wildest 1% were excluded for legibility), GS pushed past  $K_c$  and the short-call premium spiked despite the calendar pulling extrinsic value toward zero; mean P&L on the top-5% paths was  $-\$176.75$ ,  $1.55\times$  the mean loss on the worst put paths. On both legs the median path stayed inside the 25–75% band and closed flat at the premium received; the short-premium trade made money on the typical path, with both legs carrying a long left tail.

The short-call leg lost asymmetrically because IV at the contract strike rose as  $t \rightarrow T$  on every path (Fig. 4). The rise was not a model artefact: it was the empirical rise of the smile wings at short maturities that the per-ticker  $\psi_{\text{NN}}$  learned from the ladder corpus. As  $(T - t)$  shrank at fixed  $\log(K/S)$ , the standardised moneyness moved further out into the wings where  $\psi_{\text{NN}}$  grew monotonically, and a Gaussian diffusion would have underpriced that wing without the inflation, since short-horizon returns carried much heavier tails than long-horizon returns, which were close to Gaussian by central-limit averaging. The level  $v_t$  contributed only a slow mean-reverting drift around  $\theta$ , so the rise was essentially a smile-shape effect at a fixed point on the surface. On the green tail  $S_t$  pushed away from the call strike, pulling the standardised moneyness further into the wing and amplifying the rise; on the red tail the leverage coupling lifted  $v_t$  at the same time as  $S_t$  fell, so the two effects added.

We decomposed the position risk into  $\Delta$ ,  $\Gamma$ , and Vega along the same paths (Supplementary Fig. S1), computed by central finite differences on the same 201-step Leisen-Reimer American pricer used for the base marks (spot bumps of  $\pm 1.5\%$  for  $\Delta$  and  $\Gamma$ ;  $\sigma$  bumps of  $\pm 0.005$  for Vega-per-1%-IV). The long-put  $\Delta$  began near  $-0.30$  and bifurcated: on the worst-5% paths it ran to  $-1$  as the put pinned

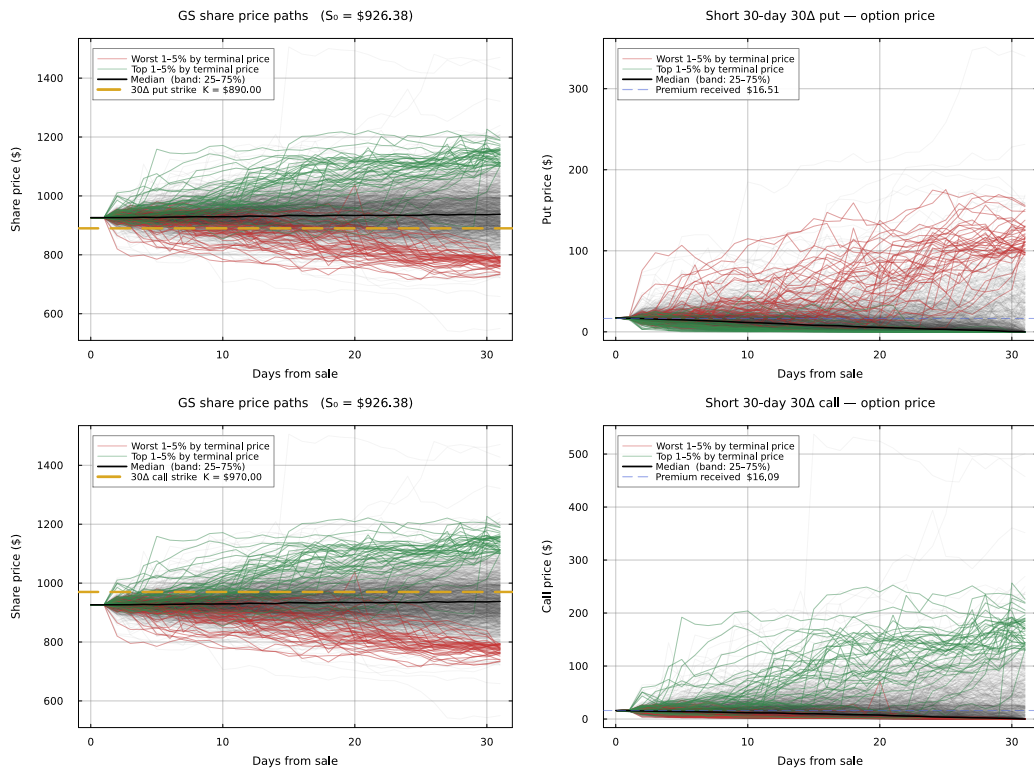


Figure 3: Forward GS share-price paths and short option premium paths for the real GS 2026-05-29 contracts, 1,000 simulated trajectories over 31 days. Top row: share path with  $K_p = \$890$  marked (left) and short-put premium (right), with the worst 1–5% by terminal price overlaid in red. Bottom row: share path with  $K_c = \$970$  marked (left) and short-call premium (right), with the top 1–5% by terminal price overlaid in green; the most extreme 1% are omitted from the overlay so the figure is not dominated by spike outliers, but the underlying summary statistics use the full top 5%. Black solid: median; shaded band: 25–75% IQR. Blue dashed lines on the option-price panels mark the market mids received at sale (\$16.51 put, \$16.09 call).

ITM at expiry, while on the rest it ran to 0; the long-call mirror image held at the call strike on the top tail.  $\Gamma$  collapsed to zero on every path that drifted away from its strike but spiked sharply on paths that pinned to the strike near expiry, the standard short-gamma signature that drives traders to avoid short-premium positions through expiry. Vega decayed monotonically toward zero on every path (the  $\sqrt{T-t}$  factor dominates), but the worst-5% put paths and top-5% call paths held materially more vega than the median through about  $t = 20$ , exposing the short-premium seller to extra IV-fluctuation risk on the same paths that were already losing on  $\Delta$ . The signs of the position-level Greeks for the short trader are the negatives of the long Greeks shown.

Both legs showed the characteristic short-premium asymmetry (Fig. 5; moments in Supplementary Table S6): a thin probability mass piled at the premium ceiling, paired with a long left tail. The short put kept its full \$16.51 premium on 72.2% of paths and closed with a mean P&L of +\$1.52; the short call kept its full \$16.09 premium on 64.3% of paths and its mean P&L of –\$9.00 was net negative, with the worst-case loss reaching –\$484.57,  $1.50 \times$  the worst put loss and  $30 \times$  the premium itself. The asymmetry between the two legs reflected the negative skew that GS’s per-ticker  $\psi_{NN}$  encodes (higher IV at down-strikes than at equally-far up-strikes) together with the leverage coupling that lifted  $v_t$  on down-paths; the put premium already reflected the down-tail risk and earned a fair return for taking it, while the call leg ran into a fatter empirical right tail than its symmetric Black–Scholes premium could cover.

We compared the simulated premium-kept rates with the trader’s delta-as-probability heuristic and found them within 3% of the rule’s prediction on both legs (Fig. 5; Supplementary Table S6). The heuristic approximates  $\Pr[\text{ITM at expiry}] \approx |\Delta|$  and so predicts premium-kept  $\approx 1 - |\Delta|$  for a

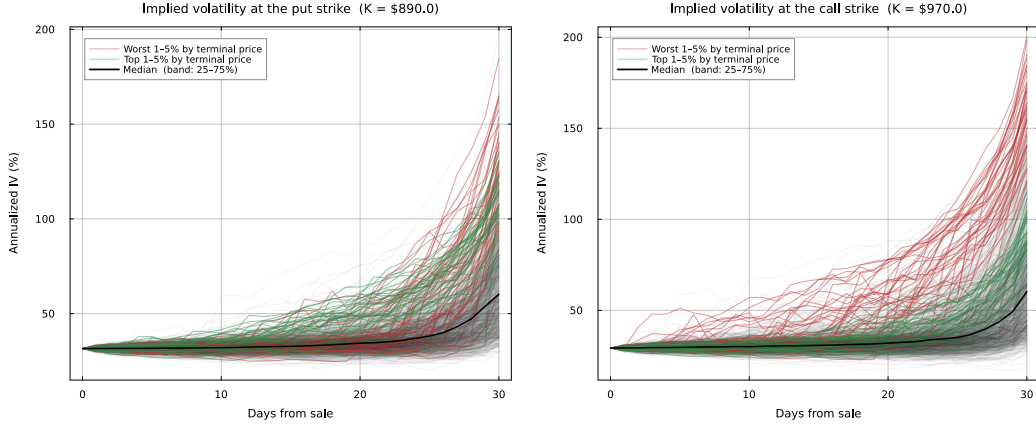


Figure 4: Path-conditional implied volatility at the put strike (left) and call strike (right) over the 31-day horizon for the GS scenario. Both panels showed IV rising into expiry: at fixed  $\log(K/S)$ , shrinking  $(T - t)$  pushed the standardised moneyness deeper into the wing of  $\psi_{NN}$ , which the per-ticker network learned to be progressively higher and steeper at short horizons. Tail-binned paths (red, green) showed an additional rise driven by  $S_t$  moving away from  $K$  and, on the put side, leverage coupling lifting  $v_t$  on down-paths.

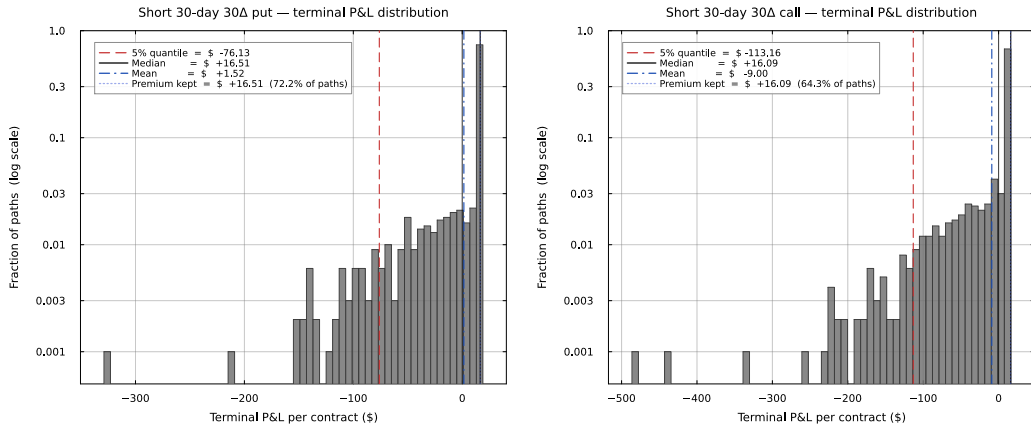


Figure 5: Terminal P&L distributions per contract (1,000 paths, log-y) for the GS scenario. Both legs showed the short-premium signature: a tall spike of paths keeping the full premium, and a long left tail. The short call’s left tail was substantially fatter than the put’s despite a smaller premium received.

short held to expiry. The GS put’s  $|\Delta| = 0.295$  implied a 70.5% rule-predicted retention against our simulated 72.2%, and the call’s  $|\Delta| = 0.328$  implied 67.2% against our 64.3% (deviations +1.7% and  $-2.9\%$ ). The agreement was a non-trivial sanity check: the rule derives from the Black-Scholes identity  $\Pr[\text{ITM}] = N(d_2) \approx N(d_1) = |\Delta|$  at short horizons and near-zero drift, while our terminal probabilities emerged from a composition of the JumpHMM marginal, Heston variance dynamics, per-ticker  $\psi_{NN}$ , and Leisen-Reimer American pricer, each calibrated to a different objective (return autocovariance, ladder RMSE, lattice convergence) and none calibrated against the rule. The directional residual—positive on the put and negative on the call—was consistent with the small positive long-run drift anchor that the JumpHMM marginal carried (Section 3): a slight upward pull lifted paths away from the put strike and toward the call strike, reducing put-side breaches and increasing call-side ones relative to a drift-free reference.

## 5.1 Cross-ticker validation: LLY

We re-ran the identical pipeline on a real LLY option pair from the same 2026-04-28 capture and observed that the model’s  $t = 0$  fair value sat \$1.35 to \$1.80 below the market mid on both legs

(Supplementary Table S7), a reversal of the near-par GS entry edges that reflected LLY’s 04-28 IV regime. The LLY pair consisted of a short put at  $K_p = \$825$  (market  $\Delta = -0.303$ , mid \$23.30, market IV 44.4%) and a short call at  $K_c = \$940$  (market  $\Delta = +0.309$ , mid \$20.76, market IV 44.0%), both expiring 2026-05-29 with LLY spot  $S_0 = \$873.83$ . Every other framework choice—the JumpHMM marginal pretrained on LLY returns, the Heston  $(\kappa, \sigma_v, \rho) = (2.0, 0.5, -0.6)$  variance dynamics, the 201-step Leisen-Reimer pricer, the per-ticker  $\psi_{NN}$  trained on the same fifteen-date ladder—was held identical to the GS scenario. LLY had dropped about 5% on 04-28 itself, so the contracts were captured against an elevated-IV market state and the per-ticker  $\psi_{NN}$  (which encodes the time-averaged shape across fifteen capture dates) sat below the realised 04-28 IV, which is why the model marked below market on both legs.

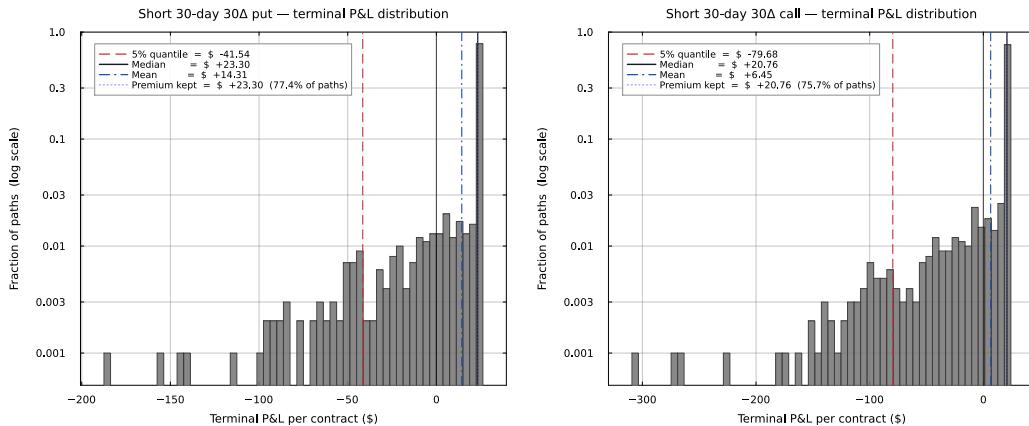


Figure 6: LLY terminal P&L distributions per contract (1,000 paths, log-y), parallel to Fig. 5. The short-premium asymmetry persisted on a ticker with substantially higher IV regime: short put kept full premium on 77.4% of paths (mean P&L +\$14.31); short call kept full premium on 75.7% of paths (mean P&L +\$6.45) with a worst-case loss of  $-\$303.88$ ,  $1.64\times$  the worst put loss and  $14.6\times$  the premium itself. Full statistics in Supplementary Table S7; share-price paths, IV trajectories, and Greek panels in Supplementary §C.

We ran the cross-ticker LLY scenario and observed that the GS result’s qualitative pattern reproduced on a ticker with materially higher IV regime—the short call carried fatter tail risk than the short put despite a smaller premium received—and a different sector with a different jump-state mixture in the JumpHMM marginal (Fig. 6; Supplementary Table S7). LLY ran at  $\sim 44\%$  market IV against GS’s  $\sim 30\%$ . Both LLY legs ran well above the delta-as-probability prediction (put: 77.4% vs rule 69.7%; call: 75.7% vs 69.1%), widening the GS-scale residual from  $\sim 3\%$  to  $\sim 7\%$  on both sides. The widened deviation was itself diagnostic: LLY’s  $30\Delta$  market deltas were computed at the elevated 04-28 capture-day IV ( $\sim 44\%$ ), while our model paths inherited the time-averaged  $\psi_{NN}$  from the fifteen-date ladder, so the model-simulated path dispersion was tighter than what the market  $|\Delta|$  implied, fewer model paths breached the strikes, and the rule-predicted ITM probability ran ahead of the simulated one. The same gap appeared at  $t = 0$  in the entry-edge column of Supplementary Table S7, where the model’s fair value sat  $\$1.35\text{--}\$1.80$  below market on both legs, the dollar-side reflection of the same  $\sim 7\%$  probability gap. The reappearance of the asymmetric-tail pattern on a second ticker showed that the negative skew came from the framework itself rather than from ticker-specific calibration choices; the widened rule deviation showed that the per-ticker  $\psi_{NN}$  was a time-averaged surface and did not adapt to single-day IV state, a property the earnings-aware extension (§4.3) addresses for scheduled events but not for unscheduled IV spikes of the kind that drove LLY’s 04-28 capture.

## 6 Discussion and Future Work

The calibration and scenario results validated the core claim of this study: a modified Heston process with a state-dependent  $\theta$ -function produced realistic IV surfaces from structural return dynamics alone, and the same decomposition of  $\theta$  into a per-ticker level and a shape function  $\psi$  accommodated a hierarchy of representations spanning a parsimonious analytic form, a globally shared

neural surrogate, and a sector-specific neural surrogate. The equilibrium initialization  $v_0 = \theta(t=0)$  eliminated  $v_0$  as a free parameter and produced the smile, skew, and term structure by construction; this was not merely a computational convenience but a structural constraint that ensured the initial IV surface was fully determined by the  $\theta$ -function, consistent with the view that IV surfaces reflect the conditional distribution of returns under the risk-neutral measure [Cont and da Fonseca \[2002\]](#). The  $\psi$ -function played an analogous role to the SVI parameterization [Gatheral \[2004\]](#) in that it provided a parsimonious representation of the smile and term structure, but with a critical difference: the parameters entered a generative model rather than a static interpolation, so the calibrated surface could evolve dynamically as the underlying HMM state changed.

Scaling the calibration to the 31-ticker fifteen-date ladder revealed the limits of the parametric form as a universal shape function and motivated the hierarchy of neural representations. A single global  $\psi$  fit across the six sectors achieved an overall RMSE of 12.48% IV (Table 1), dominated by systematic misfits in sectors whose smile geometry departed from the semiconductor baseline (technology at 15.58%, healthcare at 13.49%; Supplementary Table S2). Replacing the parametric form with a globally shared neural  $\psi$  reduced the overall RMSE to 11.47% without changing the sharing granularity, confirming that part of the gap was a functional-form bottleneck in the log-polynomial representation. Loosening the sharing to one network per sector reduced the overall RMSE further to 10.24%, with the sector NN dominating the shared NN in every sector, which established that both axes (capacity and granularity) contributed independently. The remaining error was concentrated in two structural sources: within-sector heterogeneity in technology and healthcare, where specific tickers (QCOM, MU, INTC, AMD, PFE, MRNA) carried idiosyncratic smile shapes not expressible by a shared sector-level  $\psi$ , and residual small-sample effects for the two healthcare tickers (PFE at 1,300 observations and BMY at 1,847) that still sat below the 2,000-observation per-ticker training threshold. Both sources are addressable through the same decomposition: the per-ticker roadmap relaxed shape sharing to the ticker level for the data-rich names, and additional capture days continued to reduce the small-sample variance for the remaining thin names.

Extending the corpus to eight capture days and running a temporal holdout reframed the generalization question more sharply than the in-sample RMSE alone could. The pooled-control sector NN trained on six days and evaluated on the next two carried a 4.99% IV generalization gap (8.05% train, 13.03% test; Table 2), which on its face suggested a substantial overfit. Excluding observations within  $\pm 3$  days of any same-sector earnings print from both train and test eliminated that gap entirely (8.02% train, 7.96% test,  $-0.06\%$  generalization gap), revealing that the architecture itself generalized faithfully out of sample and that the entire 4.99% gap was attributable to scheduled corporate events embedded in the holdout window. Adding earnings-distance and same-sector peer-distance features to the shape network closed roughly one fifth of the gap on the original train and test rows (11.98% test,  $+4.36\%$  generalization gap). The per-ticker decomposition exposed the mechanism (Supplementary Table S5): the peer-coupling feature carried the IV-spillover signal, so QCOM (own print six days after the window) and AMD (twelve days after) saw  $\sim 4\%$  IV reductions in test error from the INTC print on a holdout day, and the same mechanism cut META, MSFT, and GOOG test RMSE by 2 to 4% IV. INTC itself was the only Tech name whose error rose under the earnings-aware fit, driven by an oversized  $+2192\%$  EPS surprise that the calendar-based indicator could not predict. The boundary was therefore sharp: the indicator captured the part of event-day IV behaviour known in advance from the calendar (pre-print IV expansion on the reporting ticker and sympathy moves on same-sector peers), but it carried no information about the post-print outcome itself when consensus was wrong. The non-earnings baseline of 7.96% test RMSE is the right reference for what the current architecture can do under faithful temporal generalization; the residual gap to the pooled 13.03% quantifies the part of the surface that requires a richer event mechanism than the calendar.

Several limitations bounded the current claims. The cross-sector partition used conventional GICS-style groupings; whether alternative groupings (mega-cap versus semiconductor within technology; pharma versus biotech within healthcare) would improve the sector-NN fit without fragmenting the corpus was an empirical question that additional data would clarify. The forward scenario analysis demonstrated the framework on real 31-DTE 30-delta GS contracts pulled from the 04-28-2026 capture and produced a coherent path-conditional risk decomposition (Leisen-Reimer American Greeks via finite differences, terminal short-premium P&L, IV trajectories, and the entry-edge gap between the model's lattice fair value and the market mid; Figs. 4 and 5; Supplementary Table S6 and Fig. S1). A cross-ticker re-run on LLY (Supplementary §C) confirmed the qualitative pattern

on a ticker with a different sector and a higher IV regime; but the validation remained limited to two tickers from a single 30-day window in a single market regime, and broader validation across sectors and volatility environments—together with a re-run of the scenarios under the sector-NN  $\psi$  for tickers without per-ticker networks—would strengthen the generalizability claim. The current scenarios also assumed no scheduled earnings event during the simulation window, which the earnings-aware calibration flagged as the dominant residual driver of test-time error; a natural extension would forward-simulate across an earnings print and quantify how the path-conditional Greek profile and terminal P&L shifted when the event-aware  $\psi$  fed the same simulation pipeline. The earnings-aware fit recovered the anticipatory portion of the event-day signal but left the surprise-driven portion uncaptured.

A natural extension restored the per-ticker tail term that the simulation pipeline already supported for forward state evolution and that the calibration omitted: replacing the operational  $\theta_i$  with  $\theta_i \cdot (1 + \gamma_i M_i^{(t)})$ , where  $M_i^{(t)}$  was the JumpHMM tail-state probability for ticker  $i$  at time  $t$  and  $\gamma_i$  was a learned per-ticker tail sensitivity, would absorb idiosyncratic IV inflation from any source whose return-side imprint already drove the HMM into a tail state, including but not limited to earnings surprises. Restoring this term required state-conditioned histories rather than observation-day surfaces, so it sat naturally at the simulation interface: the calibrated  $\psi_{\text{NN}}$  remained the IV shape function, the calendar-based earnings inputs ( $e$ ,  $e^{\text{peer}}$ ) remained the scheduled-event indicator, and  $\gamma_i M_i$  became the unscheduled tail mechanism populated from the JumpHMM at simulation time. The natural reference point for evaluating either of these extensions was the non-event 7.96% test RMSE established by the earnings-aware calibration (Table 2), against which any further improvement would represent a genuine reduction in the residual event signal rather than a recovery of cross-sectional fit already accounted for by the sector  $\psi$ . Beyond these specific limitations, the primary intended use of this framework was generating realistic synthetic training data for machine-learning models in finance, with applications ranging from training option price predictors and learning delta-hedging policies via reinforcement learning [Buehler et al. \[2019\]](#) to augmenting scarce real option data for transfer learning. The framework naturally supported computation of Greeks ( $\Delta$ ,  $\Gamma$ ,  $\mathcal{V}$ ,  $\Theta$ ) via finite differences on the binomial-tree pricer, and the GS scenario showed that the Leisen-Reimer variant produced smooth Greeks at modest tree depth where CRR’s recombining lattice exhibited node-snapping aliasing in  $\sigma$  and  $S$  bumps. Including these Greeks in the synthetic dataset would support hedging applications. Finally, the current mood mechanism created correlated IV dynamics through a shared stress signal; a richer model could introduce ticker-pair IV correlations through the copula structure, producing a full cross-asset IV surface that respected observed correlation patterns between individual-name and index volatility.

## 7 Conclusion

In this study, we developed a framework for generating synthetic American option prices with self-consistent implied volatility dynamics. The framework linked a Jump Hidden Markov Model to a modified Heston stochastic variance process via a state-dependent mean-reversion target  $\theta(t)$ , and priced the resulting IV through a CRR binomial tree with early exercise. The equilibrium initialization  $v_0 = \theta(t=0)$  eliminated the initial IV surface as a free parameter, and the endogenous market mood signal produced correlated IV spikes during stress events without external data.

We calibrated the smile and term-structure shape function  $\psi$  through a hierarchy of representations on a 31-ticker, fifteen-date, six-sector option ladder. The five-parameter parametric form served as the analytic baseline; replacing it with a globally shared neural surrogate and then with sector-specific neural surrogates reduced the overall fit error by 8% and 18% respectively (Table 1), with independent contributions from added model capacity and loosened sharing granularity. A temporal holdout on an eight-day subset of the same capture further showed that scheduled earnings events accounted for the entire test-time generalization gap of the sector NN, and that adding calendar-derived earnings-distance and same-sector peer-distance features to  $\psi$  recovered roughly one fifth of that gap (Table 2); the residual portion arose from earnings surprises whose direction and magnitude could not be inferred from the calendar alone. We then exercised the calibrated framework as a synthetic-data generator on a real GS 2026-05-29 \$890 put and \$970 call (both 31 DTE, 30-delta) pulled from the 04-28-2026 capture, forward-simulated 1,000 price paths under the JumpHMM and the per-ticker  $\psi_{\text{NN}}$ , and tracked path-conditional implied volatility, premium decay, finite-difference Leisen-Reimer Greeks, and terminal short-premium P&L from a single coherent simulation. The

short put and short call kept their full premium on 72% and 64% of paths respectively, and the asymmetric tail risk of the short call (worst-case loss  $1.50\times$  that of the short put despite a smaller premium received; Supplementary Table S6, Fig. 5) emerged naturally from the negative skew that the per-ticker  $\psi_{NN}$  encoded together with the leverage coupling that lifted  $v_t$  on down-paths. A cross-ticker re-run on LLY (Fig. 6, Supplementary Table S7) reproduced the same qualitative asymmetry on a ticker with a different sector and a higher IV regime, confirming the result was structural rather than ticker-specific. The framework was implemented as an open-source Julia package and is available at <https://github.com/varnerlab/heston-implied-volatility-model>.

## References

- A. Alswaidan and J. D. Varner. Hybrid hidden markov model for modeling equity excess growth rate dynamics: A discrete-state approach with jump-diffusion. *arXiv preprint arXiv:2603.10202*, 2026.
- L. Andersen. Simple and efficient simulation of the Heston stochastic volatility model. *Journal of Computational Finance*, 11(3):1–42, 2008. doi: 10.21314/JCF.2008.189.
- C. Bayer and B. Stemper. Deep calibration of rough stochastic volatility models. *arXiv preprint arXiv:1810.03399*, 2018.
- F. Black and M. Scholes. The pricing of options and corporate liabilities. *Journal of Political Economy*, 81(3):637–654, 1973. doi: 10.1086/260062.
- M. Broadie and J. Detemple. American option valuation: New bounds, approximations, and a comparison of existing methods. *Review of Financial Studies*, 9(4):1211–1250, 1996. doi: 10.1093/rfs/9.4.1211.
- H. Buehler, L. Gonon, J. Teichmann, and B. Wood. Deep hedging. *Quantitative Finance*, 19(8): 1271–1291, 2019. doi: 10.1080/14697688.2019.1571683.
- R. Cont. Empirical properties of asset returns: stylized facts and statistical issues. *Quantitative Finance*, 1(2):223–236, 2001. doi: 10.1080/713665670.
- R. Cont and J. da Fonseca. Dynamics of implied volatility surfaces. *Quantitative Finance*, 2(1): 45–60, 2002. doi: 10.1088/1469-7688/2/1/304.
- J. C. Cox, S. A. Ross, and M. Rubinstein. Option pricing: A simplified approach. *Journal of Financial Economics*, 7(3):229–263, 1979. doi: 10.1016/0304-405X(79)90015-1.
- S. Demarta and A. J. McNeil. The  $t$  copula and related copulas. *International Statistical Review*, 73 (1):111–129, 2005. doi: 10.1111/j.1751-5823.2005.tb00254.x.
- E. Derman and I. Kani. Riding on a smile. *Risk*, 7(2):32–39, 1994.
- B. Dupire. Pricing with a smile. *Risk*, 7(1):18–20, 1994.
- J. Gatheral. A parsimonious arbitrage-free implied volatility parameterization with application to the valuation of volatility derivatives. Presentation at Global Derivatives & Risk Management, Madrid, 2004.
- P. Glasserman. *Monte Carlo Methods in Financial Engineering*. Stochastic Modelling and Applied Probability. Springer, 2004. doi: 10.1007/978-0-387-21617-1.
- P. S. Hagan, D. Kumar, A. S. Lesniewski, and D. E. Woodward. Managing smile risk. *Wilmott Magazine*, pages 84–108, September 2002.
- S. L. Heston. A closed-form solution for options with stochastic volatility with applications to bond and currency options. *The Review of Financial Studies*, 6(2):327–343, 1993. doi: 10.1093/rfs/6.2.327.
- B. Horvath, A. Muguruza, and M. Tomas. Deep learning volatility: a deep neural network perspective on pricing and calibration in (rough) volatility models. *Quantitative Finance*, 21(1):11–27, 2021. doi: 10.1080/14697688.2020.1817974.

- R. Jarrow and A. Rudd. Approximate option valuation for arbitrary stochastic processes. *Journal of Financial Economics*, 10(3):347–369, 1982. doi: 10.1016/0304-405X(82)90007-1.
- D. P. J. Leisen and M. Reimer. Binomial models for option valuation—examining and improving convergence. *Applied Mathematical Finance*, 3(4):319–346, 1996. doi: 10.1080/13504869600000015.
- Y. Tian. A modified lattice approach to option pricing. *Journal of Futures Markets*, 13(5):563–577, 1993. doi: 10.1002/fut.3990130509.
- M. Wiese, R. Knobloch, R. Korn, and P. Kretschmer. Quant GANs: Deep generation of financial time series. *Quantitative Finance*, 20(9):1419–1440, 2020. doi: 10.1080/14697688.2020.1730426.

## A Sector-NN calibration: corpus partition and per-sector breakdown

We decomposed the headline three-way RMSE comparison along two axes and observed that the ETF and Technology sectors together carried roughly three-quarters of the corpus, the sector NN reduced RMSE in every sector over the shared NN with the largest gains in ETF and financials, and the per-ticker residual error concentrated on a small set of technology and healthcare names (Tables S1, S2, S3). The corpus partition that defined the sector grouping is reported in Table S1, the per-sector RMSE decomposition in Table S2, and the per-ticker fit ranking under the sector NN in Table S3.

Table S1: Sector partition of the 31-ticker ladder. Each ticker appeared on at least one of fifteen capture dates (2026-04-14 through 2026-05-11); per-sector observation counts were pooled across dates. ETF observation counts were substantially larger than other sectors because SPY, QQQ, and IWM carried far deeper strike ladders than individual-name chains.

Sector	Observations	Tickers
ETF	102,738	IWM, QQQ, SPY
Technology	68,334	AAPL, AMD, AVGO, GOOG, INTC, META, MSFT, MU, NVDA, QCOM
Healthcare	26,387	ABBV, AMGN, BMY, JNJ, LLY, MRNA, PFE, UNH
Financials	17,938	BAC, GS, JPM, WFC
Retail	11,320	TGT, UPS, WMT
Energy	7,832	CVX, OXY, XOM

Table S2: Per-sector RMSE (% IV) across the three calibration strategies on the 31-ticker ladder. The sector NN reduced RMSE in every sector over the shared NN, with the largest absolute gains in ETF and financials, where the global shape poorly represented the local geometry. Healthcare and technology retained the largest residual errors, reflecting within-sector smile heterogeneity that a single shared sector  $\psi$  could not absorb.

Sector	Parametric	Shared NN	Sector NN	Obs. count
ETF	10.54	8.69	6.10	102,738
Financials	9.05	7.79	6.70	17,938
Energy	9.36	8.24	7.88	7,832
Retail	11.73	10.23	9.50	11,320
Healthcare	13.49	12.71	12.53	26,387
Technology	15.58	15.31	14.47	68,334

Table S3: Best and worst individual ticker fits under the sector-specific NN calibration, ranked by RMSE across all 31 tickers. The best fits were dominated by the broad-market ETFs and the deep-liquidity financials (GS, JPM); the worst fits were concentrated in technology (QCOM, MU, INTC, AMD) and healthcare (PFE, MRNA), where within-sector smile heterogeneity was largest. PFE and BMY remained the only tickers below the 2,000-observation per-ticker threshold.

Rank	Ticker	Obs. count	RMSE (% IV)	Sector
<i>Best 5</i>				
1	GS	8,772	5.40	Financials
2	SPY	42,224	6.02	ETF
3	IWM	21,368	6.11	ETF
4	QQQ	39,146	6.17	ETF
5	JPM	3,720	6.18	Financials
<i>Worst 5</i>				
27	PFE	1,300	17.66	Healthcare
28	AMD	4,566	17.74	Technology
29	INTC	3,417	17.78	Technology
30	MU	6,619	18.45	Technology
31	QCOM	3,375	21.46	Technology

### A.1 Leave-one-date-out validation on the fifteen-date corpus

We held out the latest capture (2026-05-11) and retrained the sector  $\psi_{\text{NN}}$  on the remaining fourteen dates as a leave-one-date-out check, and observed that the held-out test RMSE landed within 0.68% IV of the pooled train RMSE (Table S4). The held-out day comprised 14,442 observations (6.2% of the corpus); we trained the six sector networks on the remaining fourteen dates using identical architecture, schedule, and seed, standardised only on the training rows so the test split could not leak through the input scaling, and evaluated test RMSE on the held-out day. The overall train RMSE of 10.21% matched the full-corpus in-sample number of 10.24% within rounding, confirming that withholding one day did not perturb the fit, and the held-out test RMSE of 10.89% left a generalization gap of only +0.68% IV pooled across all six sectors. The gap was strongly sector-specific: four of six sectors (ETF, Financials, Healthcare, Tech) carried negative or small-positive gaps, while Energy (+2.23%) and Retail (+3.96%) showed larger positive gaps consistent with the small per-sector sample sizes on the holdout day amplifying single-name idiosyncrasies. The overall pattern was consistent with the temporal-holdout result of §4.3: with no earnings prints inside the holdout, the sector NN generalized to an unseen capture date with  $\sim 7\%$  relative degradation in RMSE, far below what an overfit model would exhibit.

Table S4: Leave-one-date-out validation of the sector NN, holding out 2026-05-11. Per-sector train and test RMSE (% IV) and gap (test – train). The pooled gap of +0.68% IV is small relative to the in-sample RMSE itself, indicating that the architecture does not overfit the fifteen-date corpus.

Sector	Train (%)	Test (%)	Gap (%)
ETF	6.12	5.87	-0.25
Financials	6.72	6.32	-0.40
Healthcare	12.58	12.00	-0.58
Tech	14.45	15.04	+0.58
Energy	7.74	9.97	+2.23
Retail	9.21	13.17	+3.96
Pooled	10.21	10.89	+0.68

## B Holdout diagnostics motivating the earnings-aware mechanism

We decomposed the holdout test error on the Tech sector across the pooled control (A) and the earnings-aware fit (C) and traced the Configuration-C improvement to the peer-coupling feature: tickers whose own prints fell outside the holdout but whose sector peers printed during it received the largest test-RMSE reductions, while INTC, the print-day ticker, was the one Tech name to worsen (Table S5). The decomposition rested on two preceding diagnostics that established the holdout RMSE jump as a localized earnings response rather than a broad-market regime shift. First, the broad-market volatility index VIX traced a flat path through the holdout window: VIX closed at comparable levels on the final training day and the two holdout days, with no intraday excursion during the holdout that approached even a one-standard-deviation move relative to the trailing six-day window. A regime-shift hypothesis required the index to move materially over the holdout, and it did not. Second, the per-ticker ATM IV trace revealed that the IV expansion on 04-23 and 04-24 was concentrated entirely in the technology sector, and within that sector concentrated on the names with earnings prints inside or adjacent to the holdout window: INTC (which printed inside the window), MSFT, META, and GOOG all exhibited ATM IV elevations of 5 to 30 percentage points relative to their training-block baselines, while non-Tech names traced ATM IV paths consistent with their pre-holdout levels. The combination established that the holdout RMSE jump was not a market-wide effect that the architecture had failed to absorb but a localized response to the earnings calendar, and it directly motivated the earnings indicator and peer-coupling feature reported in Configuration C of Table 2. INTC, the print-day ticker, was the one Tech name to worsen under the earnings-aware fit because its +2192% EPS surprise produced a post-print IV crush that no calendar-based indicator could anticipate.

Table S5: Per-ticker test RMSE on the Tech sector across the pooled control (A) and the earnings-aware fit (C). Columns  $e$  and  $e^{\text{peer}}$  report the median signed days-to-earnings and the minimum same-sector peer distance for each ticker on the holdout days. The largest gains accrued to tickers whose peers printed within the holdout (QCOM, AMD, META, MSFT, GOOG); INTC, the print-day ticker, was the one name that worsened, reflecting an unanticipated outcome that no calendar-based indicator could absorb.

Ticker	$e$	$e^{\text{peer}}$	A: pooled (%)	C: earnings-aware (%)	$\Delta$ (%)
QCOM	+5	1	41.66	37.59	-4.07
AMD	+11	1	40.07	36.50	-3.57
META	+5	1	14.32	10.73	-3.59
MSFT	+5	1	14.00	10.73	-3.28
GOOG	+5	1	9.87	7.90	-1.97
MU	-30	1	16.95	15.59	-1.36
AAPL	+6	1	10.42	10.34	-0.08
AVGO	+30	1	12.58	12.83	+0.24
NVDA	+26	1	9.43	10.47	+1.05
INTC	-1	5	33.17	35.94	+2.77

### C Short-premium scenarios: P&L statistics and cross-ticker validation

We tabulated the moments and tail statistics per contract for the GS 31-day forward simulation and observed the short-premium asymmetry that the main-text figures rendered qualitatively: a thin-tailed right side with a hard ceiling at the entry premium, paired with a long left tail that extended an order of magnitude beyond the median (Table S6). The model’s  $t = 0$  Leisen-Reimer fair value sat essentially at the market mid on both contracts (entry edge +\$0.75 on the put, -\$0.02 on the call), confirming the per-ticker  $\psi_{\text{NN}}$  matched the 04-28 GS market IV. The dispersion was larger on the call leg (std \$51.58 vs. \$34.12), and the worst-case loss on the call (-\$484.57) exceeded the worst put loss (-\$323.42) by a factor of 1.50, despite the call collecting a smaller entry premium.

Table S6: Terminal P&L statistics from 1,000 GS 31-day forward simulations of the real 2026-05-29 \$890 put and \$970 call. Entry premium was the market mid from the 2026-04-28 capture (GS spot  $S_0 = \$926.38$ ). The model’s  $t = 0$  Leisen-Reimer fair value at NN-IV was reported as a reference; statistics are per contract.

Statistic	Short put (\$)	Short call (\$)
Strike $K$	890	970
Market mid (entry premium)	+16.51	+16.09
Model $t = 0$ fair value	+17.26	+16.07
Entry edge (model - market)	+0.75	-0.02
Mean P&L	+1.52	-9.00
Median P&L	+16.51	+16.09
Std P&L	34.12	51.58
5%-tile P&L	-76.13	-113.16
Worst-case P&L	-323.42	-484.57
Premium kept in full	72.2%	64.3%

We re-ran the GS pipeline verbatim on an LLY option pair from the same 04-28 capture and observed that the qualitative features (tall premium-ceiling spike, long left tail, fatter short-call wing, leverage-driven Vega expansion on down-paths) reproduced on a ticker with a different sector, IV regime, and JumpHMM marginal (Table S7; Figs. S2, S3, S4). Terminal P&L statistics per contract are reported in Table S7; the share-price-and-premium panel (Fig. S2), IV trajectories (Fig. S3), and Leisen-Reimer American Greek panels (Fig. S4) parallel the GS figures in §5.

---

**Algorithm 2** Path-conditional Greeks via central finite differences on the LR pricer
 

---

**Require:** State  $(S, \sigma, \tau)$  with  $\tau = T - t$ ; contract  $(K, r)$ ; LR depth  $N_{LR}$ ; spot bump  $h_S$  (relative); IV bump  $h_\sigma$  (absolute).

**Ensure:**  $\Delta, \Gamma, \text{Vega}$ .

1:  $P_+^S \leftarrow \text{LR}_{N_{LR}}(S(1 + h_S), K, \sigma, \tau, r)$

2:  $P_-^S \leftarrow \text{LR}_{N_{LR}}(S(1 - h_S), K, \sigma, \tau, r)$

3:  $P_0 \leftarrow \text{LR}_{N_{LR}}(S, K, \sigma, \tau, r)$

4:  $P_+^\sigma \leftarrow \text{LR}_{N_{LR}}(S, K, \sigma + h_\sigma, \tau, r)$

5:  $P_-^\sigma \leftarrow \text{LR}_{N_{LR}}(S, K, \sigma - h_\sigma, \tau, r)$

6:  $\Delta \leftarrow \frac{P_+^S - P_-^S}{2 h_S S}$

7:  $\Gamma \leftarrow \frac{P_+^S - 2 P_0 + P_-^S}{(h_S S)^2}$

8:  $\text{Vega} \leftarrow \frac{P_+^\sigma - P_-^\sigma}{2 h_\sigma}$

▷ per unit IV; multiply by 0.01 for per-1% IV

9: **return**  $(\Delta, \Gamma, \text{Vega})$

---

Table S7: Terminal P&L statistics from 1,000 LLY 31-day forward simulations of the real 2026-05-29 \$825 put and \$940 call. Entry premium was the market mid from the 2026-04-28 capture (LLY spot  $S_0 = \$873.83$ ). LLY had dropped  $\sim 5\%$  on 04-28, so the contracts were captured against an elevated-IV regime relative to the fifteen-date calibration window; the model's  $t = 0$  Leisen-Reimer fair value at the per-ticker  $\psi_{NN}$ -implied IV came in below the market mid on both legs, with the entry edges reflecting the gap.

Statistic	Short put (\$)	Short call (\$)
Strike $K$	825	940
Market mid (entry premium)	+23.30	+20.76
Model $t = 0$ fair value	+21.95	+18.96
Entry edge (model – market)	–1.35	–1.80
Mean P&L	+14.31	+6.45
Median P&L	+23.30	+20.76
Std P&L	23.75	36.81
5%-tile P&L	–41.54	–79.68
Worst-case P&L	–185.19	–303.88
Premium kept in full	77.4%	75.7%

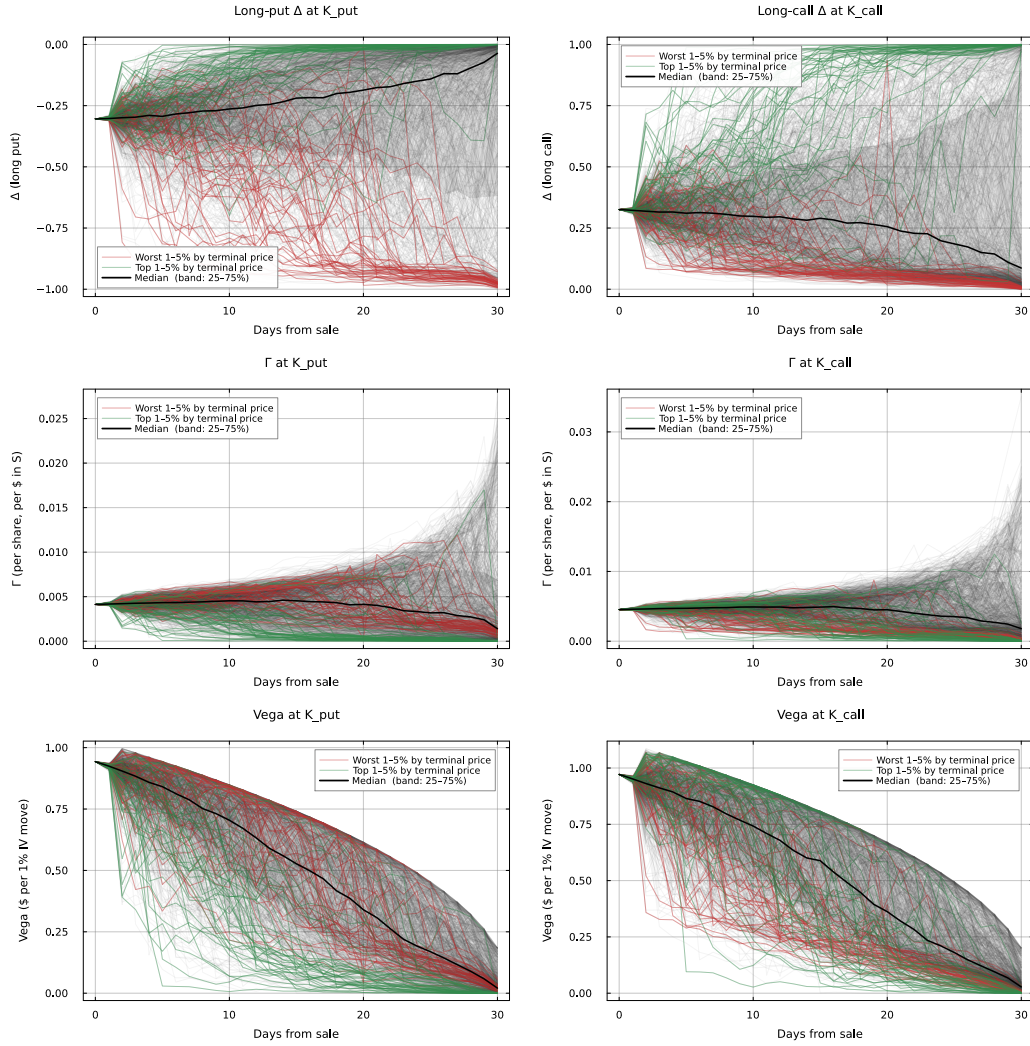


Figure S1: Leisen-Reimer American Greeks ( $\Delta$ ,  $\Gamma$ , Vega) at the GS put and call strikes over the 31-day horizon, computed by central finite differences (Algorithm 2) on the 201-step Leisen-Reimer pricer at the per-path NN-IV ( $h_S = 1.5\%S_t$  for  $\Delta/\Gamma$ ,  $d\sigma = \pm 0.005$  for Vega). Long-Greek convention: short-position Greeks are the negatives. Top row:  $\Delta$ . Middle:  $\Gamma$ , exhibiting the short-gamma spike on paths that pinned to the strike near expiry. Bottom: Vega, decaying toward zero with  $\sqrt{T-t}$  on every path. Tail overlays as in Fig. 3.

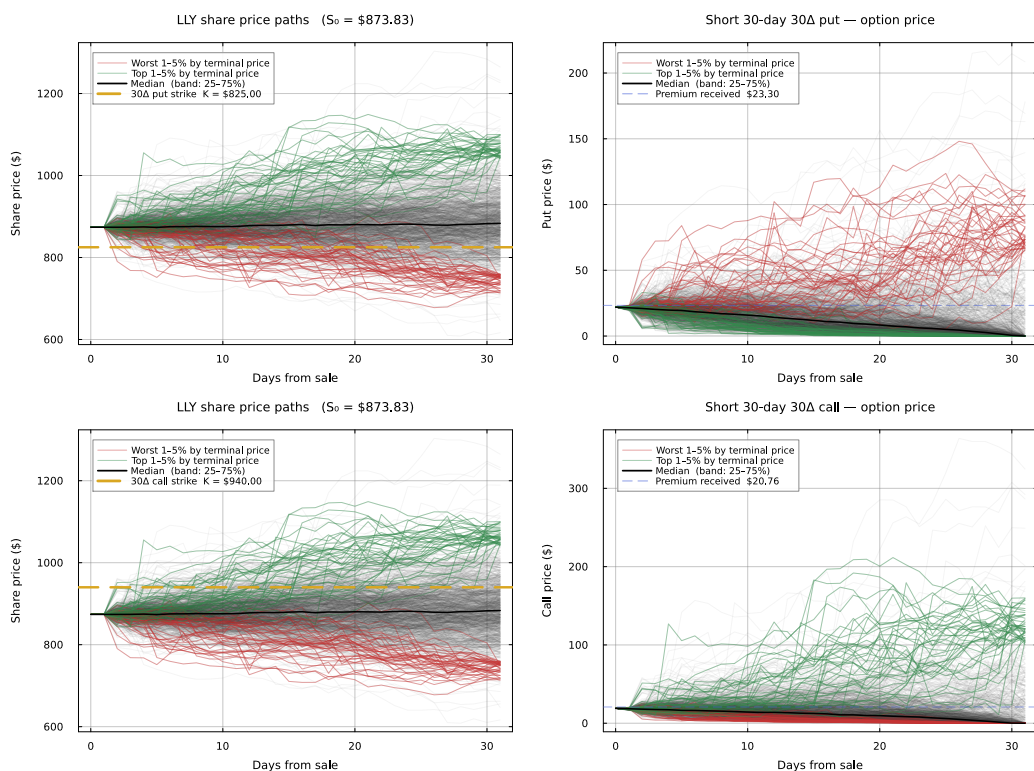


Figure S2: Forward LLY share-price paths and short option premium paths for the real LLY 2026-05-29 contracts, 1,000 simulated trajectories over 31 days; analogue of GS Fig. 3. Top row: share path with  $K_p = \$825$  marked (left) and short-put premium (right), with the worst 1–5% by terminal price overlaid in red. Bottom row: share path with  $K_c = \$940$  marked (left) and short-call premium (right), with the top 1–5% overlaid in green. The  $K_p = \$825$  strike sat  $\sim 6\%$  below spot, further from ATM than the GS put because LLY’s higher IV regime placed the same-delta strike further from spot. Black solid: median; shaded band: 25–75% IQR. Blue dashed lines on the option-price panels mark the market mids received at sale (\$23.30 put, \$20.76 call).

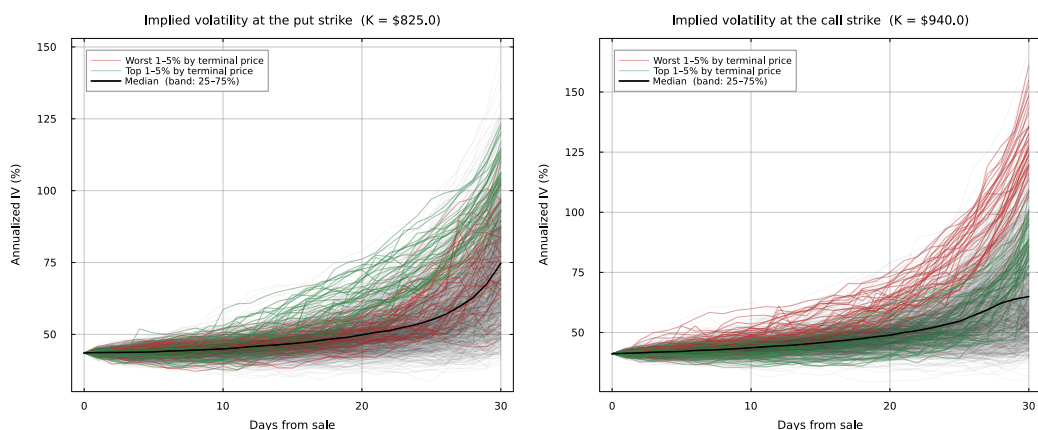


Figure S3: Path-conditional IV at  $K_{\text{put}}$  and  $K_{\text{call}}$  over the 31-day horizon; analogue of GS Fig. 4. IV expanded on worst-5% down-paths and contracted on top-5% up-paths, consistent with the negative leverage coupling  $\rho = -0.6$  that lifted  $v_t$  when shares fell.

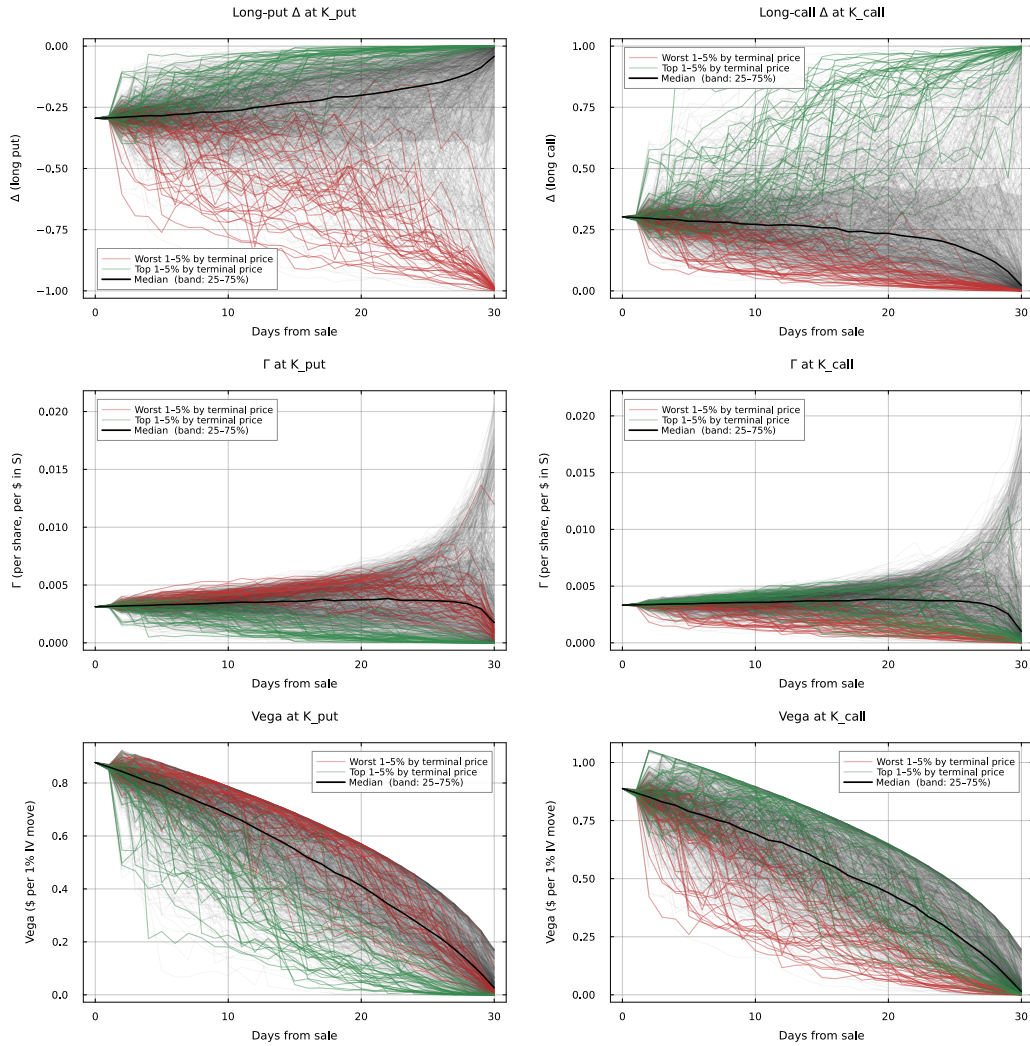


Figure S4: Leisen-Reimer American Greeks ( $\Delta$ ,  $\Gamma$ , Vega) at the LLY put and call strikes; analogue of GS Fig. S1. Short-position Greeks are the negatives of the displayed long-side values. The short-gamma spike near expiry and the  $\sqrt{T-t}$  Vega decay both reproduced the GS signatures.